AD-A038 188 DREXEL UNIV PHILADELPHIA PA F/G 21/5

IMPACT BEHAVIOR OF POLYMERIC MATRIX COMPOSITE MATERIALS.(U)

DEC 76 P C CHOU, R W MORTIMER F33615-73-C-5102

UNCLASSIFIED AFML-TR-76-242 NL

1 OF 1

AD A038188

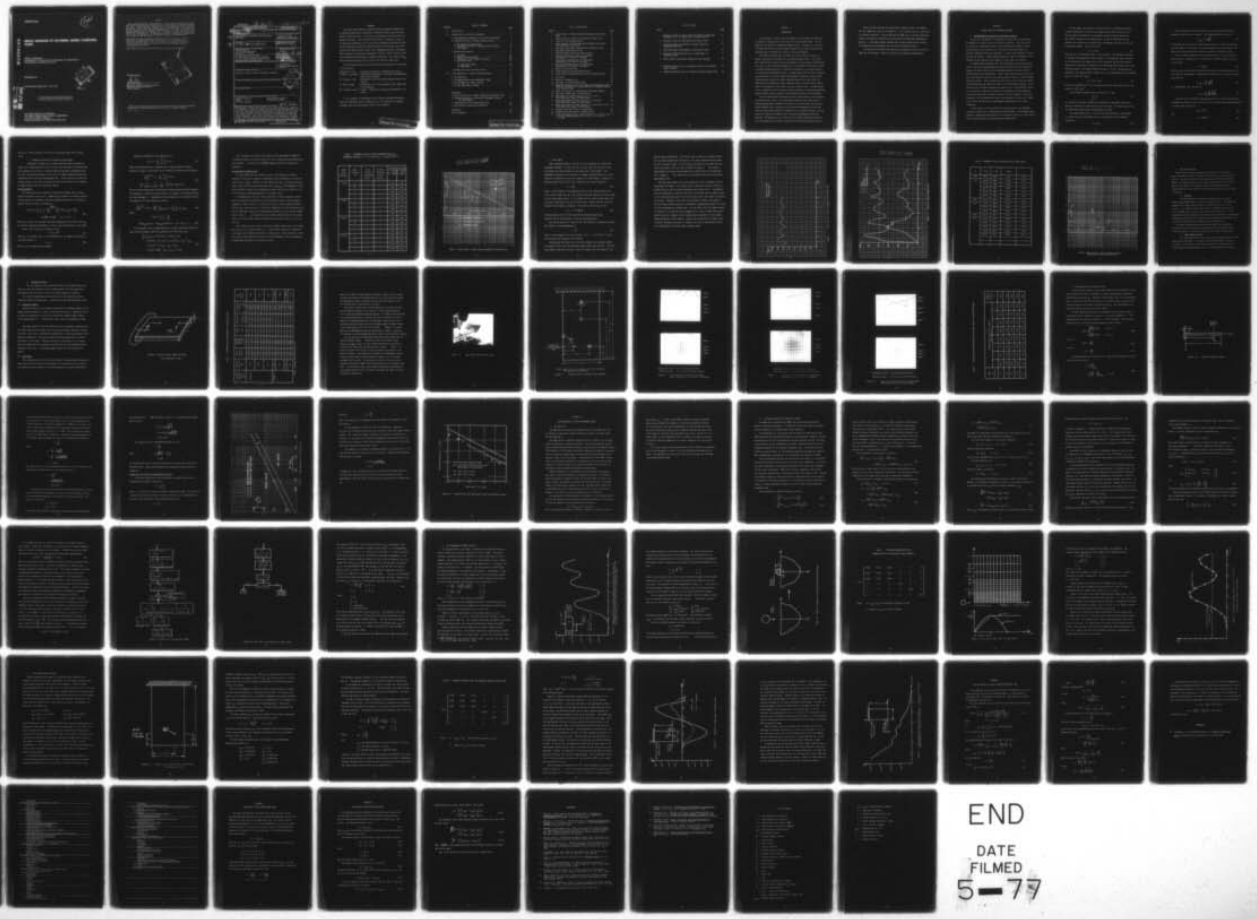

END

DATE FILMED 5-77

AFML-TR-76-242

(12)
B.S.

IMPACT BEHAVIOR OF POLYMERIC MATRIX COMPOSITE PLATES

DREXEL UNIVERSITY
DEPARTMENT OF MECHANICAL ENGINEERING AND MECHANICS
PHILADELPHIA, PENNSYLVANIA 19104

DECEMBER 1976

FINAL REPORT MARCH 1975 - JULY 1976

Approved for public release; distribution unlimited

AIR FORCE MATERIALS LABORATORY
AIR FORCE WRIGHT AERONAUTICAL LABORATORIES
AIR FORCE SYSTEMS COMMAND
WRIGHT-PATTERSON AIR FORCE BASE, OHIO 45433

NOTICE

When Government drawings, specifications, or other data are used for any purpose other than in connection with a definitely related Government procurement operation, the United States Government thereby incurs no responsibility nor any obligation whatsoever; and the fact that the government may have formulated, furnished, or in any way supplied the said drawings, specifications, or other data, is not to be regarded by implication or otherwise as in any manner licensing the holder or any other person or corporation, or conveying any rights or permission to manufacture, use, or sell any patented invention that may in any way be related thereto.

This report has been reviewed and cleared for open publication and/or public release by the appropriate Office of Information (OI) in accordance with AFR 190-17 and DODD 5230.9. There is no objection to unlimited distribution of this report to the public at large, or by DDC to the National Technical Information Service (NTIS).

This technical report has been reviewed and is approved for publication.

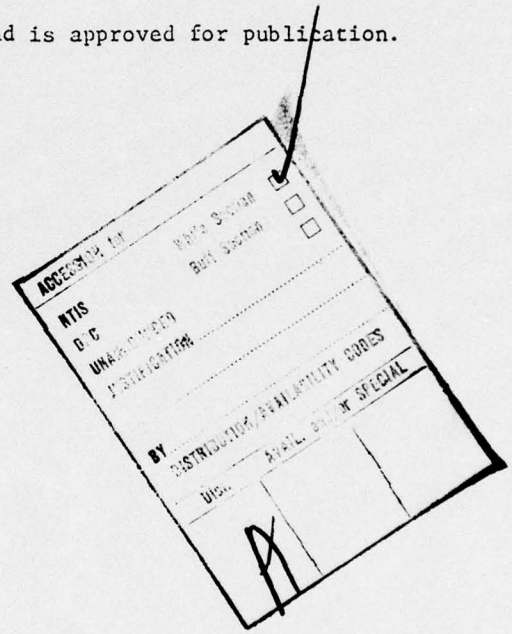

FOR THE DIRECTOR

S. W. TSAI

S. W. TSAI, Chief
Mechanics & Surface Interactions Branch
Nonmetallic Materials Division
Project Engineer

Copies of this report should not be returned unless return is required by security considerations, contractual obligations, or notice on a specific document.

AIR FORCE - 30 MARCH 77 - 200

UNCLASSIFIED

SECURITY CLASSIFICATION OF THIS PAGE (When Data Entered)

(9) Final Technical Rept. Mar 75 - Jul 76

REPORT DOCUMENTATION PAGE

READ INSTRUCTIONS BEFORE COMPLETING FORM

(18) (19) 1. REPORT NUMBER: AFML-TR-76-242

2. GOVT ACCESSION NO.

3. RECIPIENT'S CATALOG NUMBER

(6) 4. TITLE (and Subtitle): IMPACT BEHAVIOR OF POLYMERIC MATRIX COMPOSITE MATERIALS

5. TYPE OF REPORT & PERIOD COVERED: Technical - Final, March 1975 to July 1976

6. PERFORMING ORG. REPORT NUMBER

(10) 7. AUTHOR(s): Pei Chi Chou ■ Richard W. Mortimer

(15) 8. CONTRACT OR GRANT NUMBER(s): F33615-73-C-5102

9. PERFORMING ORGANIZATION NAME AND ADDRESS
Drexel University
32nd and Chestnut Streets
Philadelphia, PA 19104

10. PROGRAM ELEMENT, PROJECT, TASK AREA & WORK UNIT NUMBERS
73420201
(16) 7342 (17) 02

11. CONTROLLING OFFICE NAME AND ADDRESS
Air Force Materials Laboratory (AFML/MBM)
Air Force Wright Aeronautical Laboratories
Wright-Patterson AFB, Ohio 45433

(11) 12. REPORT DATE: Dec■■■ 76

13. NUMBER OF PAGES: 94 (12) 93 P.

14. MONITORING AGENCY NAME & ADDRESS (if different from Controlling Office)

15. SECURITY CLASS. (of this report): Unclassified

15a. DECLASSIFICATION/DOWNGRADING SCHEDULE

16. DISTRIBUTION STATEMENT (of this Report)

Approved for public release; distribution unlimited.

17. DISTRIBUTION STATEMENT (of the abstract entered in Block 20, if different from Report)

DDC RELEASE APR 7 1977 DDC

18. SUPPLEMENTARY NOTES

19. KEY WORDS (Continue on reverse side if necessary and identify by block number)

Composite materials
Impact
Structural response
Finite-difference method
Foreign-object damage

405 723

20. ABSTRACT (Continue on reverse side if necessary and identify by block number)

The problem of foreign-object impacts of jet-engine fan-blades is studied by two approaches. First, the overall response of a blade-like structure is predicted by a one-degree-of-freedom impact model in which the blade is treated as a cantilever beam or plate. Design curves are presented for finding the peak stress levels in many impact situations, including both hard and soft (fluid) impactors. Second, the local response to an edge impact is studied using a finite-difference method based on anisotropic constitutive relations. In addition, experiments have been conducted to compare with each method.

DD FORM 1 JAN 73 1473 EDITION OF 1 NOV 65 IS OBSOLETE

UNCLASSIFIED

SECURITY CLASSIFICATION OF THIS PAGE (When Data Entered)

FOREWORD

This report was prepared by Drexel University, Mechanical Engineering and Mechanics Department, Philadelphia, Pennsylvania 19104, under Air Force Contract F33615-73-C-5102. The principal investigators are Pei Chi Chou and Richard W. Mortimer. The Air Force Project Monitor is Stephen W. Tsai, of the Mechanics and Surface Interactions Branch, Nonmetallic Materials Division, Air Force Materials Laboratory, Wright-Patterson Air Force Base, Ohio 45433. Research was conducted under Project 7342, "Fundamental Research in Macromolecular Materials and Lubrication Phenomena," Task No. 734002, "Studies on the Structure-Property Relationship of Polymeric Materials." This report covers work performed during the period 15 March 1975 through 15 March 1976.

The following personnel of Drexel University participated in the research of this project:

Professor P.C. Chou - principal investigator, coordinated the project.
Professor R. Mortimer - co-principal investigator, supervised the experimental phase of the research.
Mr. William J. Flis - contributed to the "Structural Response" phase of the research.
Mr. Robert Croman - contributed to the "Local Response" phase (ANEL Code) of the research.
Mr. H. Miller and Mr. P. Kirsch - conducted the laboratory experiments of the project.

It is a pleasure to acknowledge the Air Vehicle Technology Department, Naval Air Development Center, Warminster, Pa., for supplying the composite specimens used in the experimental phase of this research.

TABLE OF CONTENTS

List of Illustrations

List of Tables

SECTION I

INTRODUCTION

In this report, we shall study the response of a jet-engine fan blade due to impacts by foreign objects, such as birds, ice and runway stones. The fan blade will be treated as a laminated composite plate. Our goal is to calculate or estimate the stress level and damage threshold in the blade and present the resulting data in a manner that can be of use to the designer.

The report is divided into two parts: the first involves structural response, and presents a procedure for constructing design curves. The second part concerns local response and the development of an anisotropic finite-difference code. In the structural-response part of the report, we shall first review a recently developed approach of treating the parameters in an impact problem in a particular non-dimensional form. A single design curve can then be applied to the same type of structure under various impact conditions. The previously published paper covered only simply supported beams, but in this report the approach will be extended to simply supported plates, cantilever plates and the effect of an impact by a soft object, such as a bird or water. A single design curve is presented for each structure and the procedure for generating additional design curves by either a numerical or experimental method is also discussed.

For the local-response calculation, either finite-element or finite-difference methods can be used. The finite-element method is more convenient for treating geometrically irregular structures; on the other hand, the finite-difference methods have a long history of solving wave-propagation problems and there are many codes available for adaption to our particular problem. Our composite fan blade can be smeared into an equivalent homogeneous anisotropic material. The geometry of the structure is then greatly simplified and therefore the problem can be handled conveniently by the finite-difference method.

There are many existing finite-difference computer codes, for example, CEL [1], TENSOR [2], HELP [3] and HEMP [4]. All of these codes are restricted to isotropic materials. We have modified the HEMP code to include anisotropic elastic constitutive relations and resulted with the ANEL code (Anisotropic Elastic). A few sample impact problems were solved by ANEL and the results are compared with experimental data and other existing solutions.

In Section II the Design Curve approach is presented; in Section III the ANEL code is described. These two sections are presented independently.

SECTION II

DESIGN CURVE FOR STRUCTURAL RESPONSE

1. Non-dimensional Parameters for Structural Response

In Ref. [5], the method for constructing a design curve for predicting the response of a given structure to impact is presented. This curve, which is in terms of a generalized strain $\bar{\varepsilon}$, and the mass ratio M (impactor mass/structure mass) can be applied to all structures of the same type but of different dimensions and various materials. It also covers impactors of different mass and velocity. Simply supported beams were used as an example in [5], although the same approach can be applied to other types of structures.

In demonstrating the method, Ref. [5] investigated six analytical models. Three of these were lumped-parameter models consisting of discrete masses and springs; the other three were distributed-mass models, which took the beam vibration modes into consideration. Some of these models neglected the contact force and treated the beam with the attached impactor mass as a free transient-vibration problem. Others included the contact-force term, traced the impactor motion distinctly, and treated the beam as a forced-vibration problem. It was shown that for the models neglecting the contact force, the generalized strain $\bar{\varepsilon}$ is a function of mass ratio M only and is independent of other parameters. For the two models which included the contact force, $\bar{\varepsilon}$ depends on M and other parameters, but the dependence on these other parameters is weak, and a single $\bar{\varepsilon}$ vs. M curve can still give an approximate representation of all impact situations.

In this report, we shall adopt two of these six models; the Timoshenko solution (or model) and a single-degree-of-freedom model. The Timoshenko model applied to simply supported plates will be reviewed in detail in a later section. Here, we shall outline the single-degree-of-freedom model.

In this model, the impactor and the structure are considered attached together immediately on contact as a lumped mass m, and the deflection of the structure is governed by an equivalent spring of spring constant K_1. The initial velocity of the combined mass, v_0, may be determined by two methods: one is based on the conservation of momentum, the other on the conservation of energy. In the first case

$$m = m_2 + em_1 \tag{1}$$

where em_1 is an "equivalent" mass of the structure. The equivalent mass may be obtained by matching the kinetic energy of the equivalent mass traveling at the velocity of the impact point in the structure and the total kinetic energy of the structure, assuming that the deflection mode shape is the static deflection curve. For simply supported beams, e = 17/35. By equating the momentum of the impactor before impact, m_2 v, with the momentum of the combined mass m, we have ($M = m_1/m_2$)

$$v_0 = v/(1 + eM). \tag{2}$$

Note that according to Eq. (2) the energy before and after impact is not conserved, or $mv_0^2 < m_2v^2$.

In the energy-conserved case, we assume e = 0, and

$$\begin{aligned} m &= m_2 \\ v_0 &= v \end{aligned} \tag{3}$$

As a result, the kinetic energy in the impactor is conserved, and will be entirely converted to strain energy in the structure. For small values of M, the difference between these two approaches is small.

The spring constant K_1 is the force per unit deflection, with respect to a force acting at the impact point in the direction of the impactor velocity, or

$$P = K_1 w_1 \tag{4}$$

After acquiring the initial velocity v_0, the mass-spring system is assumed to perform a free vibration. The maximum deflection is then

$$w_{1_{max}} = v_0 \sqrt{\frac{m}{K_1}} \quad . \tag{5}$$

In replacing the structure by a mass-spring system, it is implied that only the first mode of the structure is retained and that its mode shape is the same as the static deflection distribution under a concentrated force.

Next, we shall consider the most critical strain ε_2 in the structure which occurs at a known point 2. Assume that a relation between ε_2 and w_1 can be found,

$$\varepsilon_2 = \frac{1}{d_{12}} w_1 \tag{6}$$

where d_{12} can be determined from the static deflection distribution, $w_1(x)$, or from static measurement. Combining eq.(5) and eq. (6), we obtain the maximum strain as

$$\varepsilon_{2\ max} = \frac{v_0}{d_{12}} \sqrt{\frac{m}{K_1}} \tag{7}$$

or, combining Eq. (1), (2) and (7),

$$\varepsilon_{2\ max} = \frac{v}{d_{12}} \sqrt{\frac{m_2}{(1+eM)K_1}} \tag{8}$$

The next step of defining a generalized strain $\bar{\varepsilon}$ is best illustrated by considering a specific type of structure. For a simply supported beam impacted at middle span, we have [5]

$$d_{12} = L^2/6h \tag{9}$$

and

$$K_1 = 48EI/L^3 \quad . \tag{10}$$

Therefore,

$$\varepsilon_{max} = \frac{v}{c_0} \frac{h}{k} \sqrt{\frac{3}{4} \frac{1}{M(1+eM)}} \tag{11}$$

where $c_0 = \sqrt{E/\rho}$, the velocity of longitudinal waves in a bar. Defining the generalized strain as

$$\bar{\varepsilon} = \varepsilon_{max} \frac{c_0}{v} \frac{k}{h} \tag{12}$$

we obtain finally,

$$\bar{\varepsilon} = \sqrt{\frac{3}{4} \frac{1}{M(1+eM)}} \tag{13}$$

which is the equation of the previously mentioned design curve.

The corresponding expressions for d_{12}, K_1 and $\bar{\varepsilon}$ for simply supported orthotropic plates, cantilever beam, and cantilever plates will be given in later sections.

2. Numerical Solution of Simply Supported Plate

The engine fan blade will be simulated by a cantilever plate later in this report. Since it is not convenient to express the deflection of a cantilever plate in explicit form, we shall depend on the one-degree-of-freedom model.

In order to study the approximation involved in using the one-degree-of-freedom model, we shall first analyze a simply supported plate, which possesses a more exact solution, the Timoshenko solution. The simply supported plates will also be used to study the approximation involved in simulating a high-speed bird impact by a low-speed hard-object impact. Both the simple one-degree-of-freedom model and the Timoshenko model will be used.

a. One-degree-of-freedom Model

A simply supported rectangular orthotropic plate under a concentrated load at the center is considered. The maximum deflection occurs at the center of the plate and the maximum strain on the surface opposite from the applied

load. It can be shown (see Appendix A) that under a mild assumption, the spring constant of the plate is

$$K_1 = \frac{P}{w_{max}} = \frac{\pi^4 \, Dx}{4 \, ab\left(\frac{a}{b}\right)^2 f_1(\eta)} \tag{14}$$

where

$$f_1(\eta) = \sum_{m=1,3,5}^{\infty} \sum_{n=1,3,5}^{\infty} \frac{1}{C_{mn}} \tag{15}$$

$$\eta = \left(\frac{a}{b}\right)^2 \sqrt{\frac{Dy}{Dx}} \tag{16}$$

and

$$C_{mn} = m^4 + 2m^2 \, n^2 \, \eta + n^4 \, \eta^2 \tag{17}$$

The strain-deflection constant d_{12} relating the strain in the x-direction with w_1 is

$$\frac{\varepsilon_x}{w_1} = \frac{1}{d_{12}} = \frac{\pi^2 h \, f_2(\eta)}{2 \, ab\left(\frac{a}{b}\right) f_1(\eta)} \tag{18}$$

where

$$f_2(\eta) = \sum_{m=1,3,5}^{\infty} \sum_{n=1,3,5}^{\infty} \frac{m^2}{C_{mn}} \tag{19}$$

Combining Eq. (14), (18) with Eq. (8), and assuming e = 0, we have

$$\varepsilon_{x_{max}} = f_2(\eta) \, h \, v \left[\frac{\rho \, h}{Dx \, M \, f_1(\eta)} \right]^{1/2} \tag{20}$$

If we define the generalized strain $\bar{\varepsilon}_x$ as

$$\bar{\varepsilon}_x = \varepsilon_{x \, max} \left(\frac{c_1}{v}\right)\left(\frac{k}{h}\right) \tag{21}$$

where c_1 is the speed of flexural waves in the x-direction $\sqrt{D_{11}/I}$, then

$$\bar{\varepsilon}_x = \frac{f_2(\eta)}{[M \, f_1(\eta)]^{1/2}} \tag{22}$$

Similarly,

$$\bar{\varepsilon}_y = \frac{f_2(\eta^{-1})}{[M \, f_1(\eta^{-1})]^{1/2}} \tag{23}$$

The $\bar{\varepsilon}_x$ vs. M curve based on eq. (22) for a particular plate will be given later.

b. Timoshenko Solution of Transverse Plate Impact

Timoshenko's approach for solving transverse impact problems on beams [6] by coupling Hertz's law of contact with the Euler beam equation has been extended to the case of a simply supported isotropic rectangular plate by Karas [7] and more recently to the case of a simply supported anisotropic laminated plate by Sun and Chattopadhyay [8]. In this section we review the salient points of the latter solution and show how it may be used to develop an impact design curve for anisotropic plates.

Solution Method

The anisotropic plate equations of Whitney and Pagano [9] are used to predict the motion of the plate. Neglecting the effects of rotatory inertia, the deflection of a symmetric cross-ply laminated plate due to a centrally applied force F(t) may be expressed as

$$w(x,y,t) = \frac{4}{m_1} \sum_m \sum_n \frac{(-1)^{\frac{m+n-2}{2}}}{\omega_{mn}} \left[\int_0^t F(\tau)\sin \omega_{mn}(t-\tau)\,d\tau\right] \cdot \sin \frac{m\pi x}{a} \sin \frac{n\pi y}{b} \qquad m.n = 1,3,5 \ldots \infty \tag{24}$$

where m_1, a, and b are the mass and planar dimensions of the plate, and ω_{mn} are natural frequencies dependent on m and n and the properties of the plate.

Hertz's law of contact is assumed to hold

$$F = k_2 \alpha^{3/2} \tag{25}$$

where k_2 is a constant and α is the indentation of the impactor relative to the plate surface, or

$$\alpha = w_2 - w \tag{26}$$

where w_2 is the impactor displacement.

Newton's law applied to the impactor m_2 is

$$w_2 = vt - \frac{1}{m_2} \int_0^t \int_0^t F \, dt \, dt \tag{27}$$

These four equations may be combined into a single nonlinear integral equation in terms of the contact force F between the plate and the impactor,

$$\left[\frac{F}{k_2}\right]^{2/3} = vt - \frac{1}{m_2} \int_0^t \int_0^t F \, dt \, dt$$

$$- \frac{4}{m_1} \sum_{m=1,3,5}^{\infty} \sum_{n=1,3,5}^{\infty} \frac{1}{\omega_{mn}} \int_0^t F(\tau) \sin \omega_{mn}(t-\tau) d\tau \tag{28}$$

which is solved numerically by applying the small-increment method suggested by Timoshenko, in which the contact force F is assumed to be constant during any time increment $\Delta\tau$. Expanding the above integrals to calculate the force F_i during the i^{th} time interval, we obtain

$$\left[\frac{F_i}{k_2}\right]^{2/3} = vn\Delta\tau - \frac{(\Delta\tau)^2}{m_2} \sum_{j=1}^{i} D_{i-j+1} F_j - \frac{4}{m_1} \sum_{j=1}^{i} F_j E_{i-j+1} \tag{29}$$

where

$$E_{i-j+1} = \sum_m \sum_n \frac{1}{\omega_{mn}^2}$$

$$\cdot \{\cos[\omega_{mn}(i-j)\Delta\tau] - \cos[\omega_{mn}(i-j+1)\Delta\tau]\}, \quad m,n = 1,3,5,\ldots,\infty \tag{30}$$

If the contact force is approximated as a linear continuous function of time, with an average value of F_i during the i^{th} time step, then

$$\sum_{j=1}^{i} D_{i-j+1} F_j = 2[(n-1)F_1 + (n-2)(F_2 - F_1)$$

$$+ (n-3)(F_3 - F_2 + F_1) + \cdots + (n-j)(F_j - F_{j-1} + F_{j-2}$$

$$- \cdots \pm F_1) + \cdots + (F_{n-1} - F_{n-2} + F_{n-3} -$$

$$\cdots \pm F_1)] + \tfrac{1}{3}(F_n - F_{n-1} + F_{n-2} - \cdots \mp F_1) \tag{31}$$

For computing the solution of Eq.(29), Sun and Chattopadhyay suggested a recursion method, but we have found that such a time-saving approximation is not necessary. A listing of our FORTRAN computer program is presented in Appendix B.

Construction of Design Curve

As can be seen from the nonlinear nature of Eq.(28), the structural response of the plate to impact is dependent on more parameters, not only the mass ratio $M = m_1/m_2$. However, we will demonstrate that, for plates of given aspect ratio (a/b) and given anisotropy ratio (D_{22}/D_{11}), the dependence of the plate response on these other parameters is weak, and that one family of $\bar{\varepsilon}$ vs. M curves gives a good approximation of all impact cases.

To determine the effect of these quantities on impact response, a parametric calculation was carried out, with different values of the following parameters: impact velocity v, contact stiffness k_2, plate bending stiffness matrix $[D_{ij}]$, and mass ratio M. The actual magnitudes of these quantities used and the calculated values of the generalized strains $\bar{\varepsilon}_x$ and $\bar{\varepsilon}_y$ are all summarized in Table I. An inspection of this table indicates that for any given value of M, the maximum difference between any two values of $\bar{\varepsilon}_x$, or of $\bar{\varepsilon}_y$, is only 12%.

This solution may be used to construct an impact design curve by plotting points on an $\bar{\varepsilon}$ vs. M graph (Figure 1). These points alone can be connected by a single curve which may be used as a design curve. Note that such a curve would not be very different from the curve corresponding to the one-degree-of-freedom model discussed in an earlier section.

Table 1 PARAMETRIC STUDY OF SIMPLY-SUPPORTED PLATES BY TIMOSHENKO SOLUTION. ($\bar{v}$ = 2.45 m/sec, $\bar{k}_2 = 1.744 \times 10^{19}$ N/m$^{3/2}$)

Mass ratio, $M=m_1/m_2$	Impact velocity, $v/\bar{v}$	Hertz contact stiffness, $k_2/\bar{k}_2$	Flexural stiffness matrix, $D_{ij}/\bar{D}_{ij}$	Generalized Strain	
				$\bar{\varepsilon}_x = \frac{\varepsilon_x S_x^2}{hv}$	$\bar{\varepsilon}_y = \frac{\varepsilon_y S_y^2}{hv}$
1.036	1	1	1	2.512	1.538
	$\sqrt{2}$	1	1	2.536	1.538
	1	2	1	2.592	1.556
	1	1	2	2.339	1.440
0.784	1	1	1	2.770	1.702
	$\sqrt{2}$	1	1	2.798	1.713
	1	2	1	2.848	1.731
	1	1	2	2.609	1.635
0.475	1	1	1	3.298	1.983
	$\sqrt{2}$	1	1	3.340	1.988
	1	2	1	3.425	1.999
	1	1	2	3.021	2.025
0.242	1	1	1	4.585	2.910
	$\sqrt{2}$	1	1	4.611	2.922
	1	2	1	4.678	2.946
	1	1	2	4.418	2.794

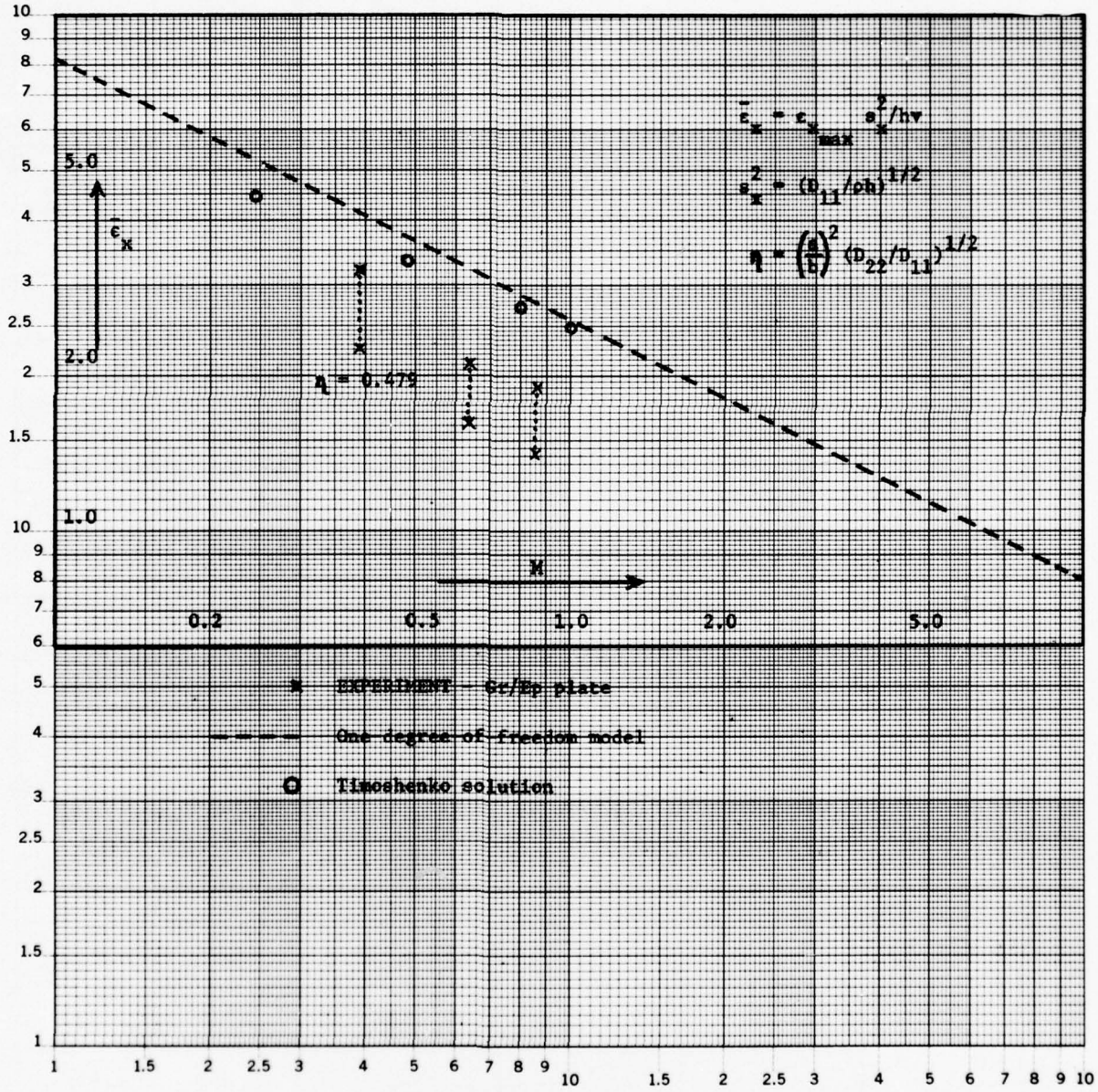

Figure 1. Central Impact of Simply Supported Rectangular Orthotropic Plate

c. Bird Impact

Under high-speed impact, the body of a bird responds as a fluid with negligible strength. In this section, we shall treat the bird as a fluid and compute the stress induced in the blade due to fluid impact. The Timoshenko solution for the response of a simply supported plate to a solid impactor was modified to treat the loading of a fluid impact. Instead of a Hertzian contact force, the force F exerted on the plate is given by

$$F = \phi A v_R^2 \tag{32}$$

where ϕ is the density of the impacting fluid, A the cross-sectional area of the fluid column, and v_R is the relative velocity between the fluid column and the plate impact point. It is assumed that the fluid column cannot sustain axial compression, and the fluid velocity v remains constant until the complete fluid column is consumed. The relative velocity v_R is then

$$v_R = v - \dot{w}\left(\frac{a}{2}, \frac{b}{2}\right) \tag{33}$$

Substituting Eqs. (32) and (33) into (24) we obtain the governing equations for w; this equation is then solved numerically.

The contact duration T, which is the time required to completely consume the column, can be approximated as

$$T = \frac{L}{v} \tag{34}$$

where L is the length of the fluid column. For $t > T$, the force F is zero and the plate will continue free vibration.

Calculations were made for two velocity regimes; the low-speed regime was around 6 m/sec, and the high-speed regime larger than 60 m/sec. The low-speed impact cases were studied in order to compare with the results of the

gelatin impact experiments. The contact time is long for low-speed impact, and the fluid loading force fluctuates a very small amount from that given by ϕAv^2, instead of ϕAv_R^2. In other words, the motion of the plate does not affect the contact force too much, as shown in Figure 2. The strain is approximately the same as that produced by a static force of the magnitude ϕAv^2, Figure 3. The results will be discussed further in the section on experimental work.

The high speed impact cases were studied in order to simulate the true high-speed bird impact. The contact time is short and the plate velocity, $\dot{w}$ becomes large so that its motion influences the contact force. A parametric study was undertaken in which M, the ratio of the plate mass to impactor mass, A, the cross-sectional area of the fluid column, and v, the impactor velocity, were varied. Results of this study are presented in Table 2 and Figure 4. As can be seen, points plotted in coordinates of generalized strain $\bar{\varepsilon}$ vs. mass ratio M are grouped in a single band. For any value of M, the largest spread of values of $\bar{\varepsilon}$ is only 34%, which suggests that a curve through these points may be useful as a design tool for predicting the response of other simply supported plates to fluid impact. Further, by conducting a few impact tests on actual fan-blade structures, a similar curve can be constructed to serve as a design guide for a wide range of impact cases.

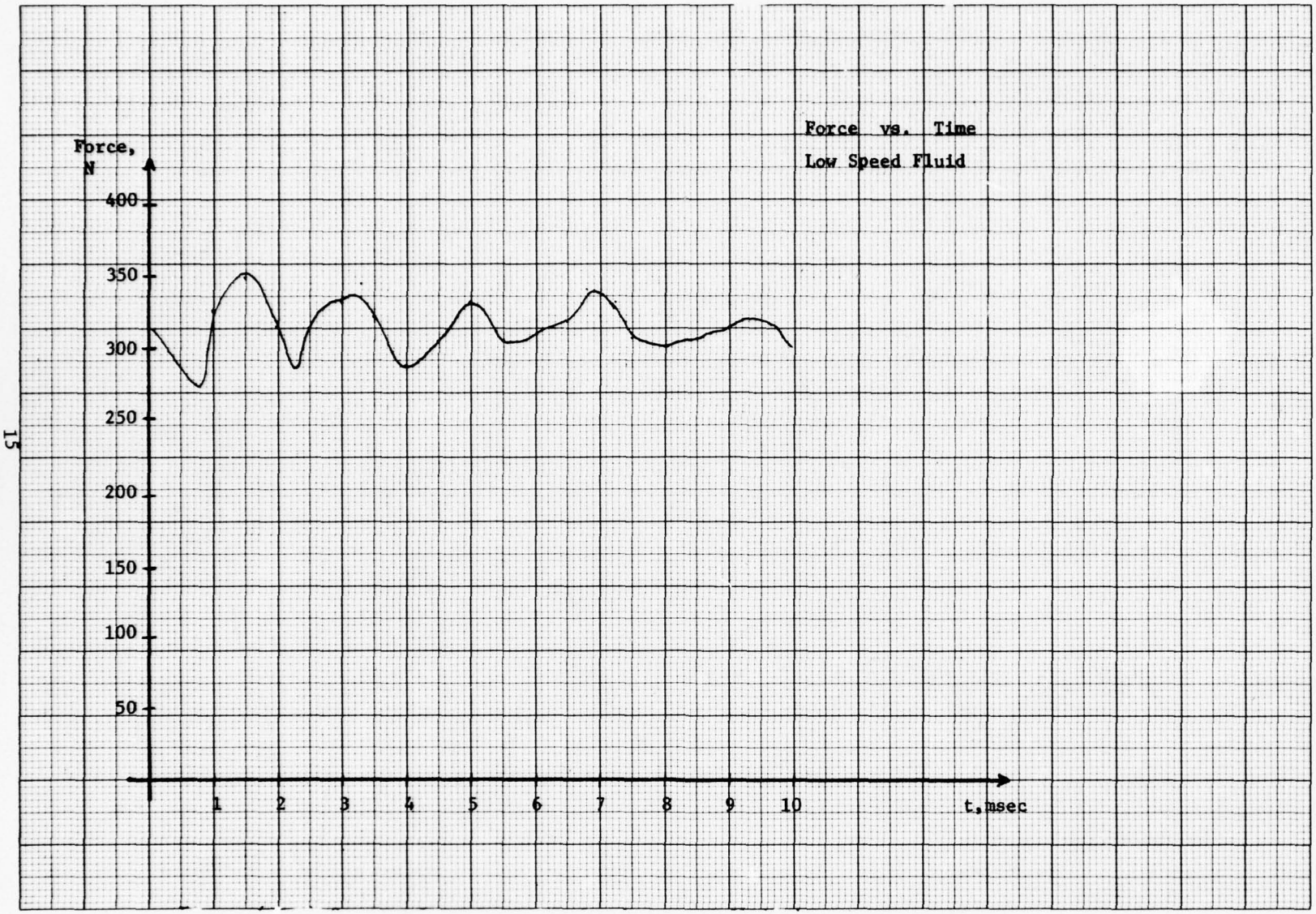

Figure 2. Contact Force vs. Time for Low-Speed Fluid Impact Case

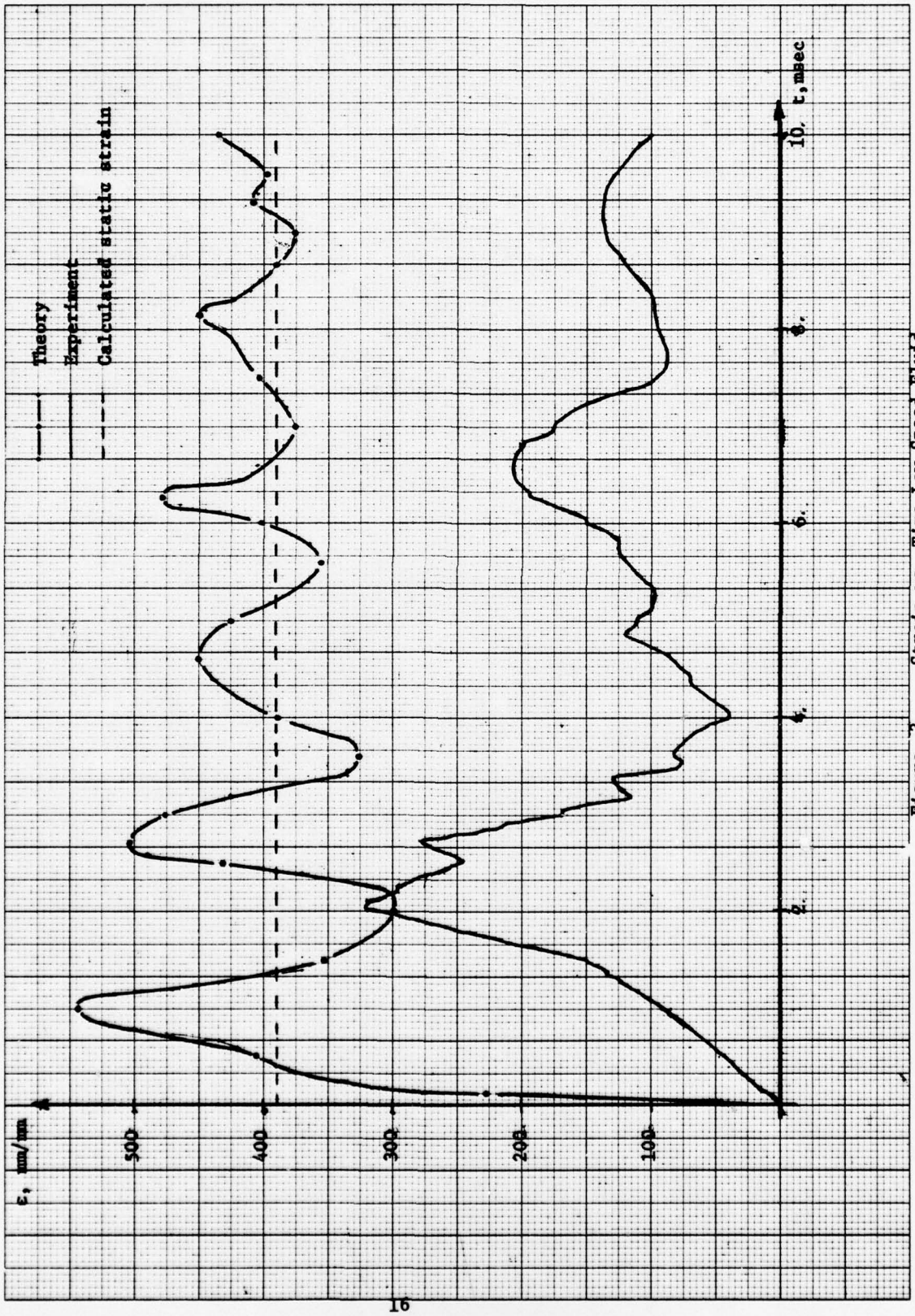

Figure 3. Strain vs. Time Low Speed Fluid

Table 2. PARAMETRIC STUDY OF HIGH-SPEED FLUID IMPACT MODEL

M	v, m/sec	A, mm^2	ε mm/mm	$\bar{\varepsilon}$
1.92	60.96	5806.	0.031	0.56
1.49	60.96	5806.	0.032	0.58
	91.44	5806.	0.058	0.71
	121.92	5806.	0.054	0.49
	152.40	5806.	0.074	0.54
	274.32	5806.	0.140	0.56
0.96	137.16	5806.	0.121	0.97
0.75	91.44	5806.	0.065	0.79
	121.92	5806.	0.105	0.95
	152.40	5806.	0.137	0.99
0.64	137.16	7903	0.133	1.07
0.49	91.44	7903	0.083	1.01
	121.92	7903	0.125	1.14
	152.40	7903	0.171	1.24
	60.96	17419	0.066	1.19
	152.40	17419	0.131	0.95

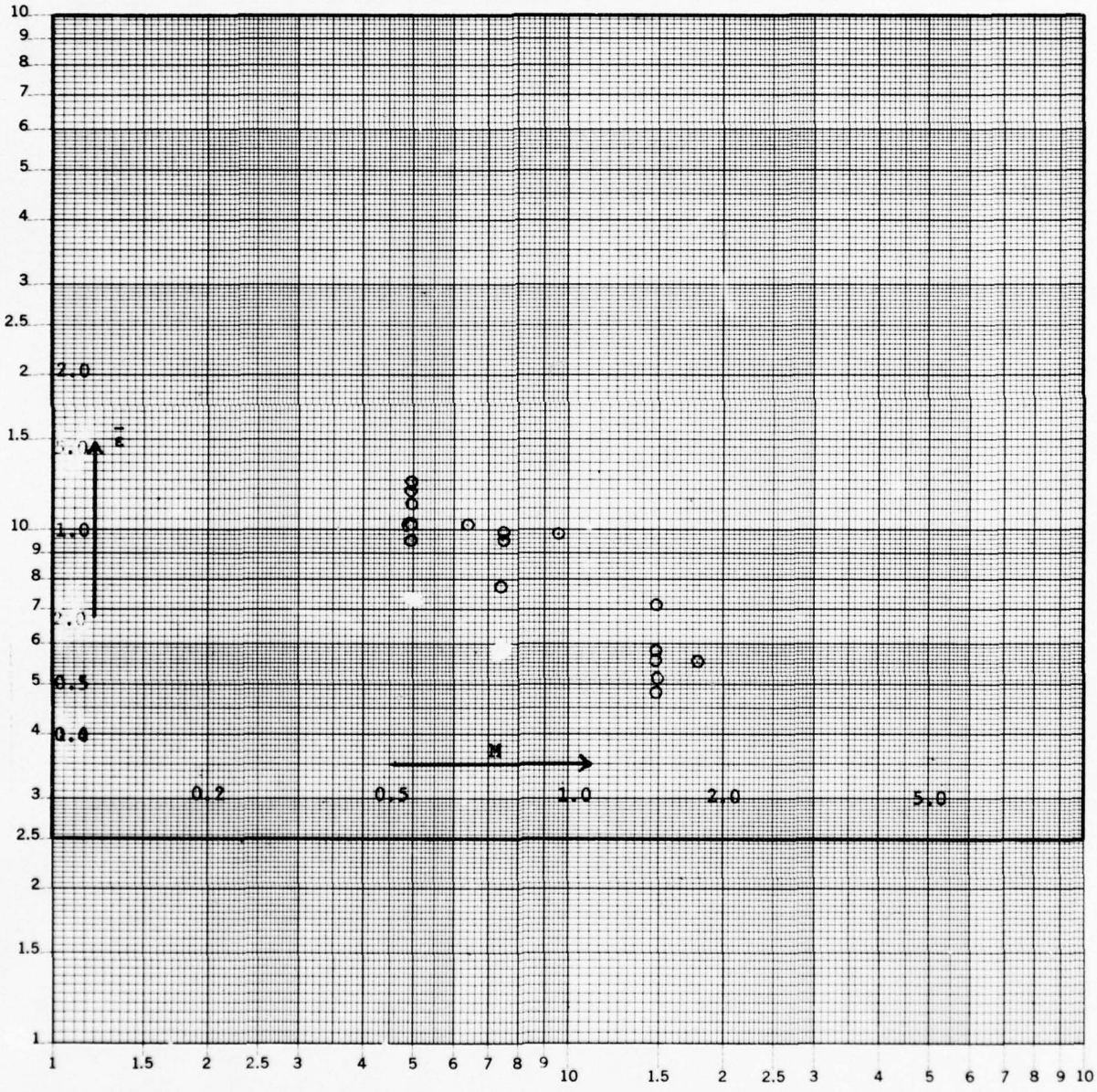

Figure 4. Central Impact of Simply Supported Rectangular Orthotropic Plate High Speed Fluid Model

3. Experimental Approach

Several series of impact experiments were conducted. All the experiments used composite plates of the same material and layup, but with different supports. One series involves a simply supported plate, the other cantilever plates. The simply supported plate was impacted transversely both by steel impactors and by gelatin. The cantilever plates were impacted by steel and aluminum impactors in the transverse direction and on the edge at various angles of incidence.

a. Specimens

All plate specimens were fabricated from Hercules, Inc., AS3501 graphite-epoxy prepreg tape, at a layup of $[(0/45/0/-45)_6/0]_S$. The dimensions and mass of the simply supported plate were 349x171x7.1 mm (a x b x h) and 0.660 kg. Two cantilever plates were tested: (1) 330x178x7.1 mm, 0.647 kg., and (2) 330x89x7.1 mm, 0.324 kg. Plate (2) was cut from plate (1). These dimensions and masses include only the supported areas of the plates; an additional 4-mm margin protruded beyond the supports around the simply supported plate, and 24 mm of the cantilever plates extended into the clamping device.

The simply supported plate and the cantilever plate were transversely impacted by blunt (25.4-mm contact radius) steel cylindrical impactors using a drop-test machine. The cantilever plate was also tested with edge impacts.

b. Simply Supported Plates

The simply supported plate was rested upon a rectangular frame of round-edged blades and impacted at the center by various impact masses at several velocities. The strain in the plate directly opposite the impact point was measured using a Micro-Measurements, Inc., type EA-41-125AD-120 strain gage,

and recorded using an Ellis BAM-1 bridge amplifier and Tektronix Type 565 oscilloscope. Impact velocity was determined from the drop height. Data from these experiments by steel impactor are summarized in Table 3. This result is also included in Figure 1.

c. Simulation of Bird Impact by Gelatin

An attempt was made to simulate high-speed bird impacts by low-speed impacts produced by dropping a gelatin mixture onto the simply supported plate. The strain in the plate was measured in the same manner as described above for the hard-object impact experiments. The gelatin mixture was prepared from food-type gelatin (e.g., Jello) according to package directions but with 75% extra water added.

After much experimentation with various devices for dropping the gelatin onto the plate, fairly repeatable results were finally obtained by the following procedure. The gelatin mixture was prepared (set) inside lengths of 2.82-inch (I.D.) plastic pipe. A smooth flat plate was firmly pressed against the bottom end of the pipe to retain the gelatin. The pipe was held above the plate specimen and the retaining plate was suddenly pulled aside, allowing the gelatin to fall. A sheet of aluminum foil, situated a small distance above the plate specimen, made contact with the plate on impact of the gelatin, completing an electrical circuit and triggering the oscilloscope for strain measurement.

In the course of these experiments, it was observed that the impact duration was longer than the calculated period of the lowest mode of plate vibration. However, in an actual high-speed bird impact, the impact duration is characteristically much shorter than the fundamental period. This large discrepancy in the kinematics of the two cases indicates that low-speed fluid impact experiments cannot be used to even approximately simulate high-speed bird impact.

Table 3. TRANSVERSE IMPACT EXPERIMENTS ON SIMPLY SUPPORTED GRAPHITE/EPOXY PLATE

Impactor mass, m_2 (kg)	Impact velocity, v (m/s)	Average maximum measured strain $\varepsilon_x \times 10^6$	Number of tests	Coefficient of variation, per cent	Generalized strain $\bar{\varepsilon}_x = \varepsilon_x \frac{s_x^2}{hv}$	Mass ratio $M=m_1/m_2$
0.816	2.45	4320	5	8.4	1.952	0.809
	2.99	4760	5	19.6	1.759	
	3.46	4960	5	13.9	1.584	
	4.23	6450	2	7.7	1.684	
	4.89	6670	3	4.3	1.507	
1.04	2.45	4320	5	8.4	1.952	0.635
	2.99	5500	2	2.6	2.032	
	3.46	5700	4	6.2	1.820	
	4.23	8200	3	9.2	2.141	
	4.89	9550	2	0.7	2.157	
1.72	2.45	6050	2	5.8	2.734	0.384
	2.99	7300	2	5.8	2.697	
	3.46	10180	5	1.9	3.250	
	4.23	12680	4	4.2	3.310	

d. Cantilever Plates

For all impacts on the cantilever plate, the specimen plates were held in a jig that provided 25 mm of clamping depth. For the edge impact experiments, the jig could be rotated to various angles of incidence.

Two series of experiments were conducted for the cantilever plates, transverse impact and edge impact. These will be described separately below.

(1) Transverse Impact

Cantilever plate (1) was impacted transversely in a manner similar to the simply supported plate, at a point 76 mm from the free end. Bending strain in the plate was measured at a point 25.4 mm from the clamped support using a strain gage (Figure 5). The results of these tests are presented in Table 4.

Cantilever plate (2) was also failure-tested by gradually increasing both the impact mass and drop height until failure was visually detected. During each test, the strain in the plate was measured by a strain gage mounted 25 mm from the clamped end. The plate finally failed when impacted by a 6.08-kg lead block at 5.99 m/sec. Failure occurred in a zone about 3 to 5 cm away from the clamped end, and apparently resulted from the high bending stresses produced in this area. Strain-measurement results are also presented in Table 4.

(2) Edge Impact

This experimental study was the first phase of an experimental analytical study which had as its goal the development of an analytical tool to predict the transient strain response of a turbine-blade-like structure subjected to

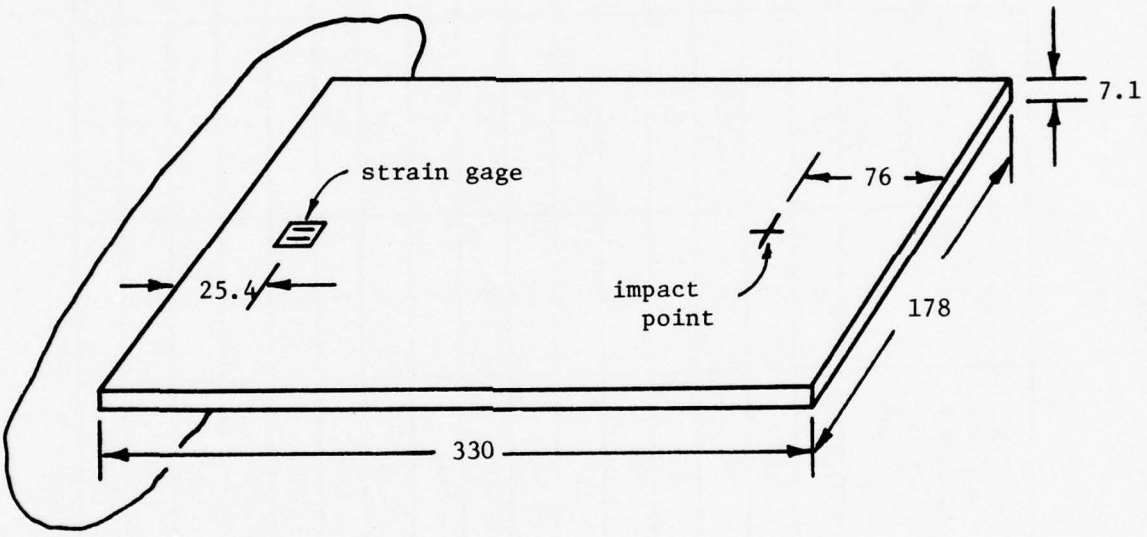

Figure 5. Cantilever Plate Impact Specimen.

(All dimensions in mm.)

Table 4. TRANSVERSE IMPACT EXPERIMENTS ON CANTILEVER PLATES

Specimen dimensions axbxh (mm)	Impactor mass, m_2 (kg)	Impact velocity, v (m/sec)	Average maximum measured strain, $\varepsilon_x \times 10^6$	Number of tests	Coefficient of variation, per cent	Generalized strain, $\bar{\varepsilon}_x = \varepsilon_x \frac{s_x^2}{hv}$	Mass ratio, $M=m_1/m_2$
330x178x7.1	0.495	2.45	523	3	1.1	0.453	1.309
		3.46	750	3	0.0	0.459	
		4.23	967	3	0.6	0.478	
	0.784	2.45	635	4	2.7	0.550	0.825
		3.46	927	3	2.5	0.568	
		4.23	1177	3	0.5	0.588	
	1.057	2.45	840	4	1.0	0.727	0.612
		3.46	1193	3	1.0	0.731	
		4.23	1447	3	0.4	0.723	
330x89x7.1	2.54	4.89	4300	1	-	1.861	0.1276
	3.29	4.23	4500	1	-	2.249	0.0985
		4.89	5000	1	-	2.164	
		5.47	5600	1	-	2.168	
	3.52	7.60	7200	1	-	2.005	0.0922
	6.08	4.89	6500	1	-	2.814	0.0533
		5.99	7800*	1	-	2.716	

* Note: Specimen failed during this test.

impact on its edge at various angles of incidence. However, due to a change in scope of this grant the analytical phase of this study was never initiated. The experimental results are presented here for reference purposes in case this proposed study is reactivated in the future.

This series of impact tests involved impacting the cantilever specimen plate (previously described) on its edge by a 0.85" (21.6mm) diameter by 1.0" (25.4mm) long aluminum cylindrical impactor. The impactor was accelerated by a low-pressure air gun to a velocity of 40 fps (12.2 m/sec); the point of impact on the specimen plate was at its 80% length. During the tests the cantilever plate was rotated such that the incident angles of impact included in this study were 0°, 22.5°, 45°, 67.5° and 90°. Figure 6 is a photograph of the experimental set-up used in these tests. Figure 7 identifies the locations of the strain gages and point of impact of the cylindrical impactor.

At least three sets of reproducible strain traces were recorded for each angle of incidence impact. Figures 8, 9, and 10 are typical strain histories of gages 4 and 9; for the 0° impact these traces are identical and for the 90° impact they are identically out of phase. Table 5 includes the values of the average of the peak strains at each gage for each angle of incidence. Also included in this Table is the experimental value of the wave velocity based on strain initiation at gages 1 and 4 as the wave propagates into the plate. As anticipated, the value of the wave velocity decreases as the impact changes from an inplane mode (0°) to a transverse mode (90°). The theoretical values of the inplane- and shear-wave velocities for this specimen plate are 0.166×10^6 in/sec (4220 m/sec) and $.0436 \times 10^6$ in/sec (1110 m/sec), respectively.

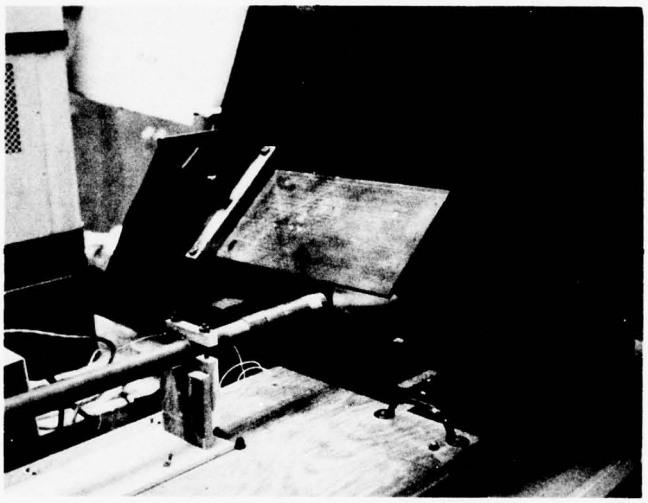

Figure 6. Edge Impact Experimental Set-up

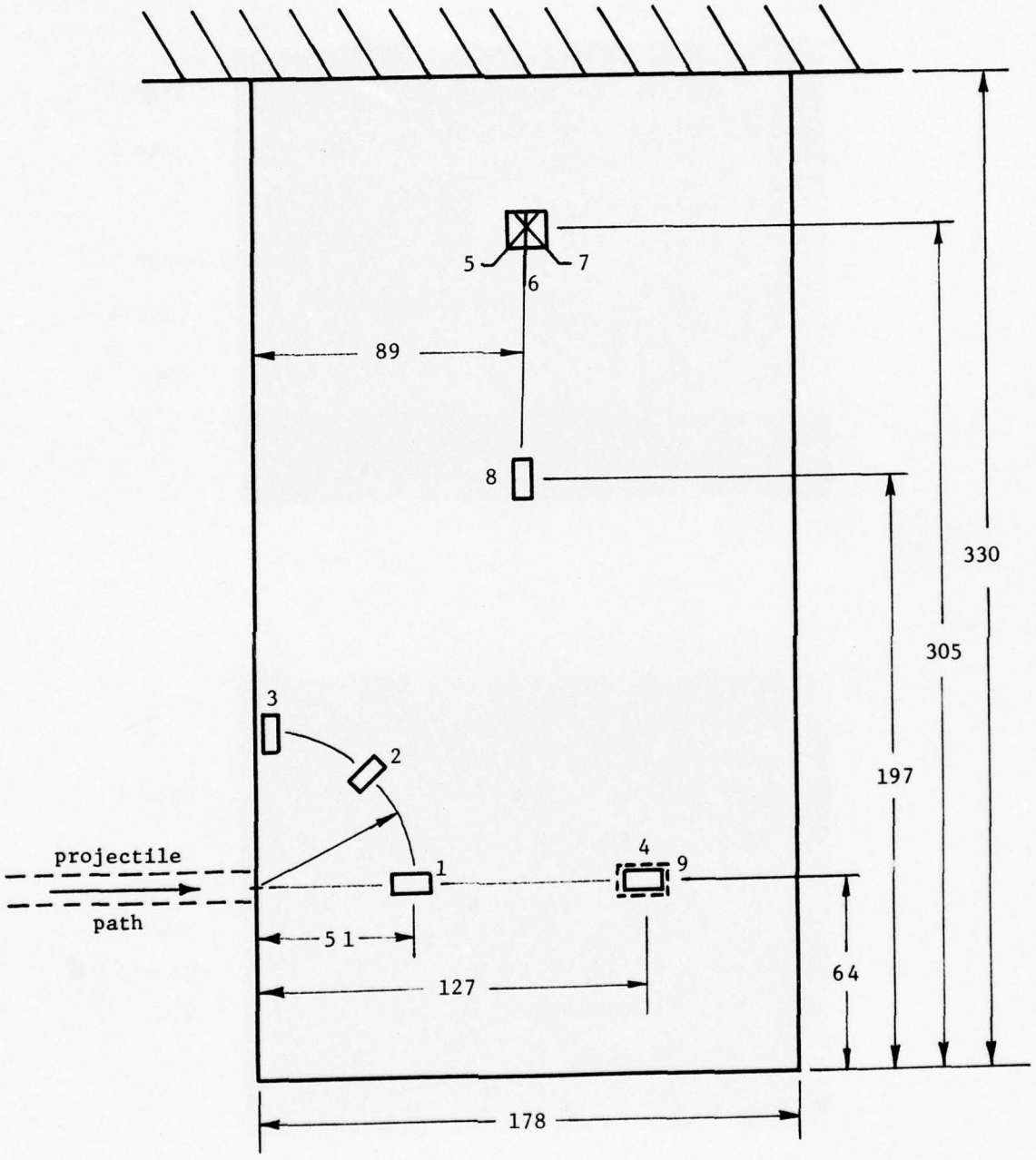

Note: Gage 9 is on top of plate; all others on bottom.
All dimensions in millimeters.

Figure 7. Specimen Geometry and Strain Gage Locations

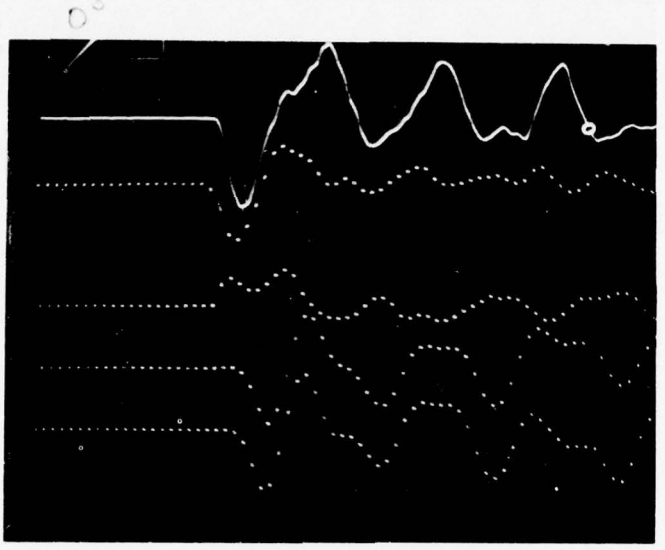

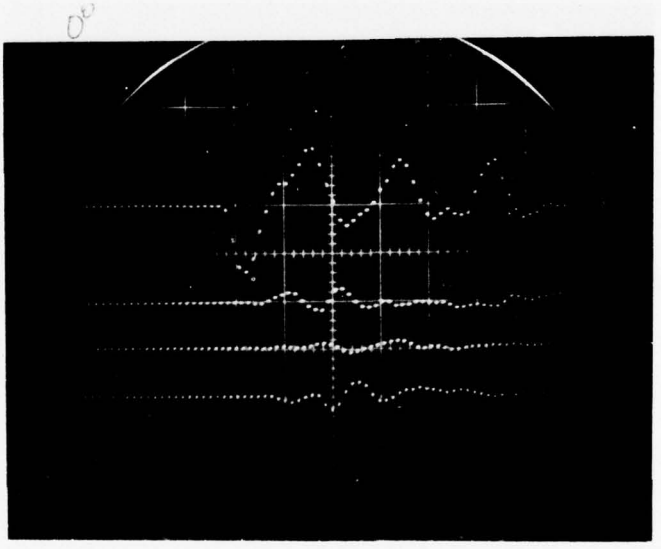

Horizontal Scales: 50 μsec per major division

Vertical Scales: 0.1% strain per major division

Figure 8. Typical Oscilloscope Traces for Edge-Impact Experiments at 0° Angle of Incidence.

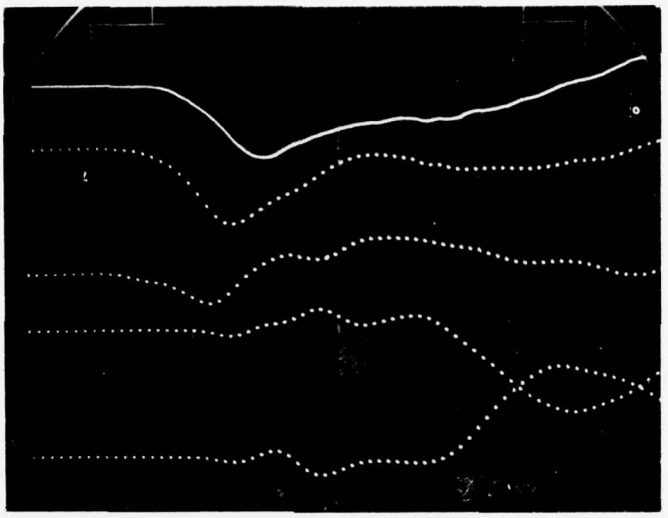

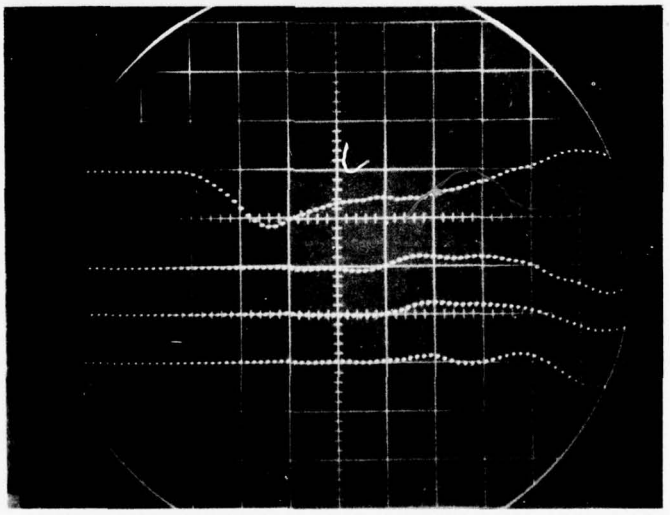

Horizontal Scales: 50 μsec per major division

Vertical Scales: 0.1 % strain per major division

Figure 9. Typical Oscilloscope Traces for Edge-Impact Experiments at 45° Angle of Incidence.

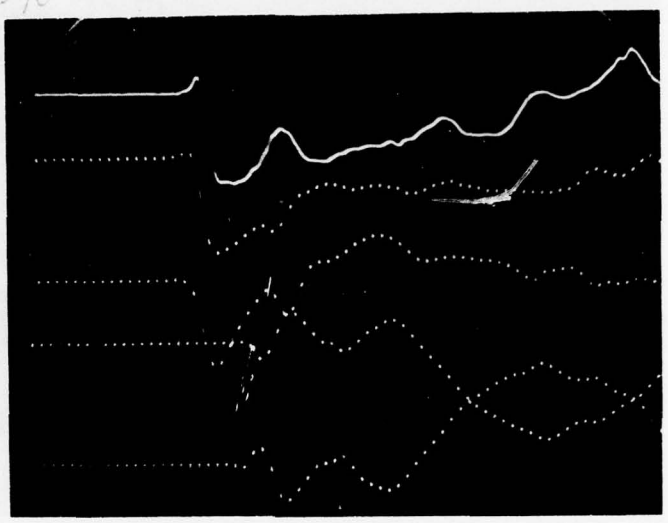

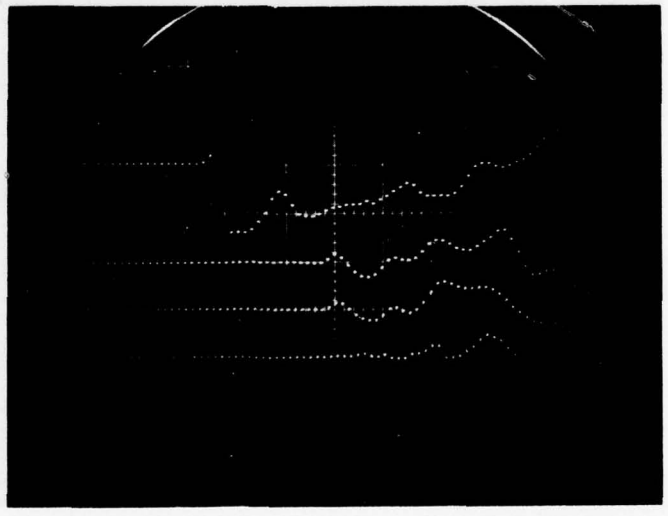

Horizontal Scales: 50 μsec per major division

Vertical Scales: 0.1% strain per major division

Figure 10. Typical Oscilloscope Traces for Edge-Impact Experiments at 90° Angle of Incidence.

Table 5. STRAINS AND WAVE VELOCITIES DUE TO EDGE IMPACT OF CANTILEVER PLATE

Angle of incidence	Maximum strain (x 10^6) at gage no. (See Figure 9)								Wave velocity (m/sec) 1 → 4
	1	2	3	4	9	5	6	7	
0°	-1500	-1025	+500	±850	±1050	+325	+225	+375	4110
22.5°	-1300	-1350	-817	-867	+1017	-383	-333	-400	4110
45°	-1400	-1517	-833	-1567	+1650	-767	-500	-700	2820
67.5°	-1383	-1517	-1000	-1867	+1850	-700	+467	-650	3050
90°	-1517	-1533	-1550	-1483	+1583	+683	+650	+467	1600

4. Design Curves for Cantilever Plate

Since the exact solution of the static deflection of orthotropic rectangular cantilever plates is not known, we cannot obtain explicit analytical expressions for K_1 and d_{12}. Instead, we shall handle this in two approximate ways. The first is to treat the plate as a cantilever beam, and use the deflection function of the beam to obtain K_1 and d_{12}. The other method is to measure K_1 and d_{12} directly from static tests.

We shall consider the plate as a cantilever beam of length L under a concentrated load P applied at a point x = d as shown in Figure 11. The expression for the strain at a point x = c will be derived. The deflection distribution of a cantilever beam subjected to such a load is

$$w_1(x) = \begin{cases} \frac{Px^2}{6EI}(3d-x) & 0 \leq x \leq d \\ \frac{Pd^2}{6EI}(3x-d) & d \leq x \leq L \end{cases} \tag{35}$$

At x = d,

$$w_1(d) = \frac{Pd^3}{2EI} \tag{36}$$

so that

$$K_1 = \frac{2EI}{d^3} \tag{37}$$

The bending strain in the beam at x = c may also be determined from the static deflection curve.

$$\begin{aligned} \varepsilon_2 &= \frac{h}{2}\left.\frac{\partial^2 w}{\partial x^2}\right|_{x=c} \\ &= \frac{h}{d^2}\left(1 - \frac{c}{d}\right)w_{1_{max}} \qquad (c \leq d) \end{aligned} \tag{38}$$

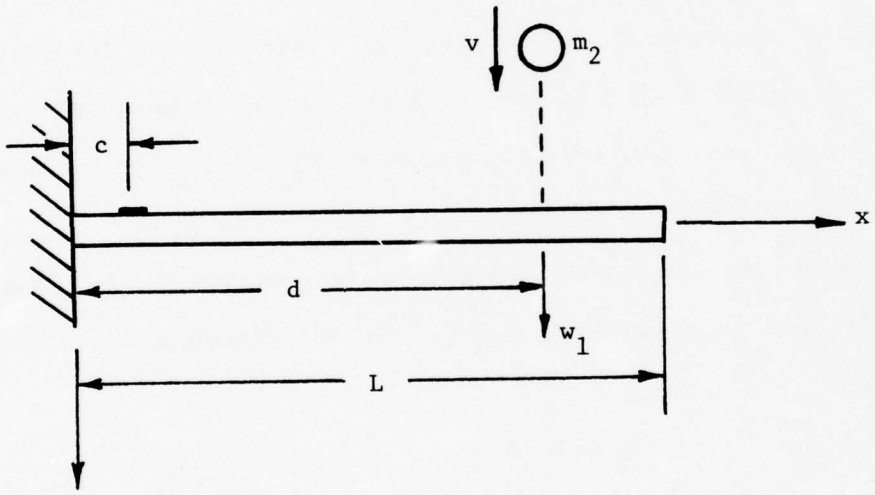

Figure 11. Impact of Cantilever Beam

Therefore

$$d_{12} = \frac{d^3}{h(d-c)} \tag{39}$$

Following the definition of $\bar{\epsilon}$ from Eq.(12), we have

$$\bar{\varepsilon} = \left(1 - \frac{c}{d}\right)\left[\frac{3}{4M(d/L)}\right]^{1/2} \tag{40}$$

In this case $\bar{\varepsilon}$ is a function not only of M but also of the parameters (d/L) and (c/d). Note that $\bar{\varepsilon}$ is a maximum at c = 0, i.e., at the supported end.

Another way of determining K_1 and d_{12} for the cantilever plate is direct static measurement of P, w_1, and ε_2. Referring to Figure 11, if a load P is applied at x = d, and the deflection w_1 at x = d and the strain ε_2 at x = c are measured, then the values of K_1 and d_{12} can be calculated from Eqs. (4) and (6).

We have made static measurements on the specimen shown in Figure 5. The results are presented in Table 6. The experimental values of K_1 and d_{12} are

$$K_1 = 49700 \text{ N/m}$$

$$d_{12} = 12.6 \text{ m}$$

Application of Design Curves to Turbine Blades

The design curve for cantilever plates and beams can be used to determine the resistance of a turbine-engine fan blade to structural failure caused by a particular impact. This will be demonstrated by means of an example.

For a blade similar to the composite cantilever plate specimen described in section II-3 (330 x 178 x 7.1 mm, 0.647 kg), it is desired to find

Table 6. STATIC TESTS ON CANTILEVER COMPOSITE PLATE SPECIMEN

Force		Deflection		Strain
lb	N	.001 in	mm	μs
0.0	0.0	0.0	0.000	0
5.0	22.2	15.6	0.396	36
10.0	44.5	33.0	0.838	72
15.0	66.7	48.7	1.237	106
20.0	89.0	65.0	1.651	140
23.1	102.6	78.0	1.981	166
25.1	111.5	84.5	2.146	178
30.1	133.7	101.4	2.576	216
35.1	156.0	119.2	3.028	252
40.1	178.2	137.0	3.480	288
44.9	199.6	153.2	3.891	316
45.1	200.4	154.3	3.919	322
49.9	221.9	170.8	4.338	352
54.9	244.1	189.3	4.808	388
59.9	266.3	208.6	5.298	428
61.9	275.2	216.1	5.489	442

the structural-failure impact velocity for a 0.54-kg bird striking the blade 76 mm from the tip. From static flexure tests, it is determined that the flexural rigidity EI is 408 N-m^2 (therefore $a^2 = \sqrt{EI/\rho A} = 14.4$ m^2/sec), and that the blade fails in bending near the supported end when the outer-fiber tensile strain reaches the value of $\varepsilon = 0.008$. With these data the design curve for the blade may be constructed. Treating the blade approximately as a cantilever beam, the equation for the curve, Eq.(40), may be written as

$$\bar{\varepsilon} = \frac{c_1}{\sqrt{M}}$$

where

$$c_1 = \left(1 - \frac{c}{d}\right)\sqrt{\frac{3L}{4d}}$$

$$= \left(1 - \frac{0}{254}\right)\sqrt{\frac{3(330)}{4(254)}}$$

$$= 0.866$$

For a mass ratio M = 1.2, the generalized strain is $\bar{\varepsilon} = 0.79$. Therefore, the normal impact velocity which will just initiate failure is

$$v = \frac{\varepsilon\, a^2}{h\, \bar{\varepsilon}}$$

$$= \frac{(0.008)(14.4)}{(0.0071)(0.79)}$$

$$= 20.5 \text{ m/sec}$$

A design curve for the blade may also be constructed by means of static strain and deflection measurements. In this case, the constants K_1 and d_{12} are determined experimentally, as discussed in the previous section. The values are found to be

$$K_1 = 49700 \text{ N/m}$$

$$d_{12} = 12.6 \text{ m}$$

for a static force applied at the impact point and for strain measured near

the supported end. Then by Eq.(8), using e = 0 (conservation-of-energy model) we have

$$v = d_{12}\ \varepsilon_{2max} \sqrt{\frac{k_1}{m_2}}$$

$$= (12.6)(0.008)\sqrt{\frac{49700}{0.54}}$$

$$= 30.6 \text{ m/sec}$$

The equation for the corresponding design curve is

$$\bar{\varepsilon} = \frac{c_2}{\sqrt{M}}$$

where

$$c_2 = \sqrt{\frac{EI\ a}{k_1}} \quad \frac{1}{d_{12}\ h}$$

$$= 0.582$$

This equation may also be used to determine the critical impact velocity as described above. These two equations for the design curve are plotted in Figure 12.

Design Curve in Terms of Dimensionless Velocity

The impact design curve may be presented in another useful form. A dimensionless velocity is defined as

$$\bar{v} = v \frac{h}{a^2\ \varepsilon_f}$$

where ε_f is the value of strain for which the structure fails. Note that when v has the value of the critical or failure velocity v_c, the dimensionless velocity is the reciprocal of the generalized strain $\bar{\varepsilon}$,

$$\bar{v}_c = \frac{1}{\bar{\varepsilon}}$$

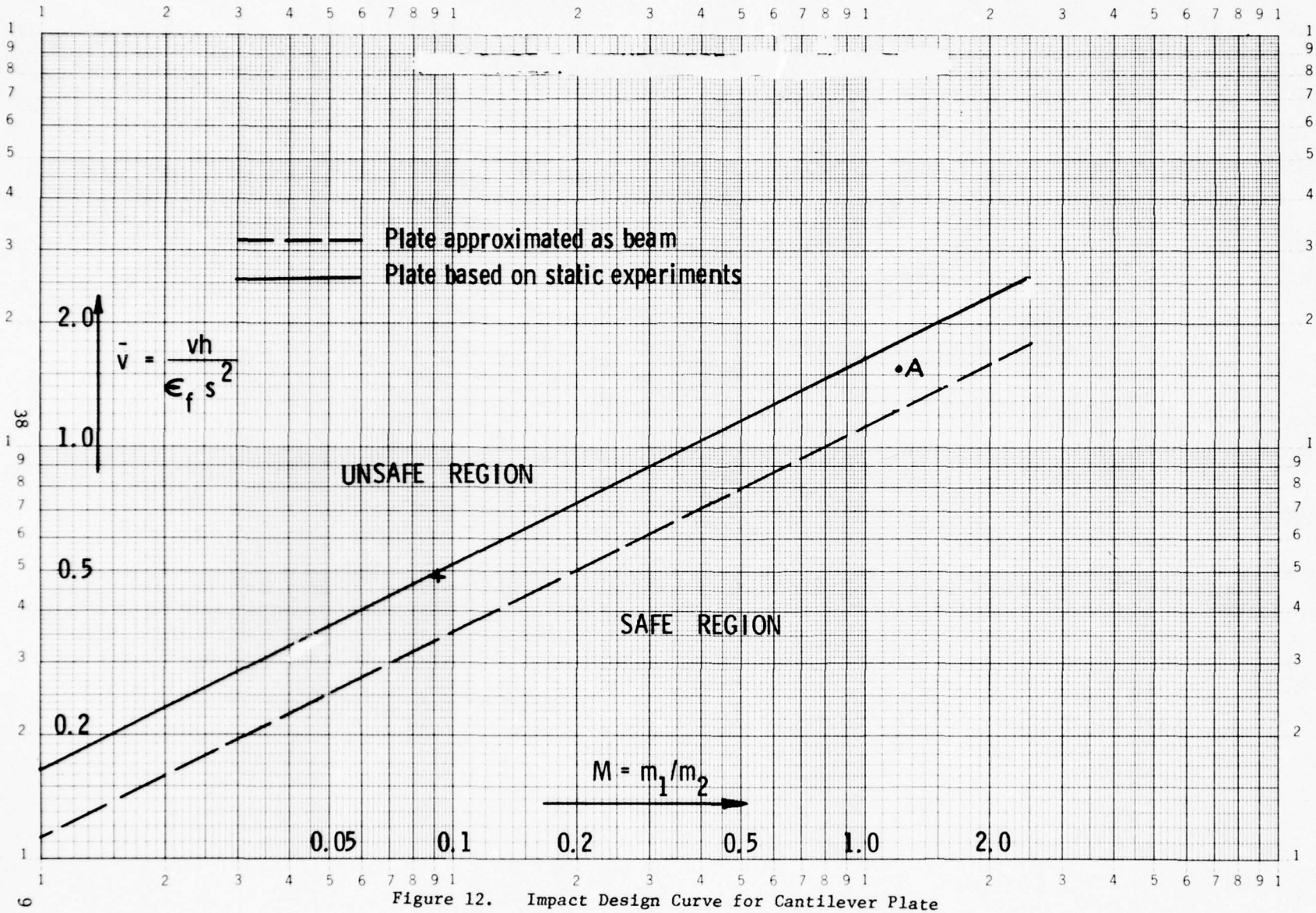

Figure 12. Impact Design Curve for Cantilever Plate

Therefore,

$$\bar{v}_c = \frac{\sqrt{M}}{C_i}$$

where the constant C_i is determined from calculations or experiment as discussed above.

If this equation is plotted in $\bar{v}$ vs. M coordinates, Figure 13, the curve will divide the plane into safe (below the curve) and unsafe (above) regions. For a particular impact situation, the values of $\bar{v}$ and M may be computed. If the point on the graph corresponding to these values falls below the curve, structural failure due to bending will not occur; if the point falls above the curve, failure will occur.

For example, it is desired to determine whether a 0.54-kg bird (M = 1.2) impacting the blade at 25 m/sec will cause failure. Computing the dimensionless velocity, we obtain

$$\bar{v} = (25)\ \frac{(0.0071)}{(14.4)(0.008)}$$

$$= 1.54$$

In Figure 12, this is plotted as point A, lying above the design curve for the cantilever beam and below the curve for the plate based on static measurements; thus, the former curve predicts failure whereas the latter does not.

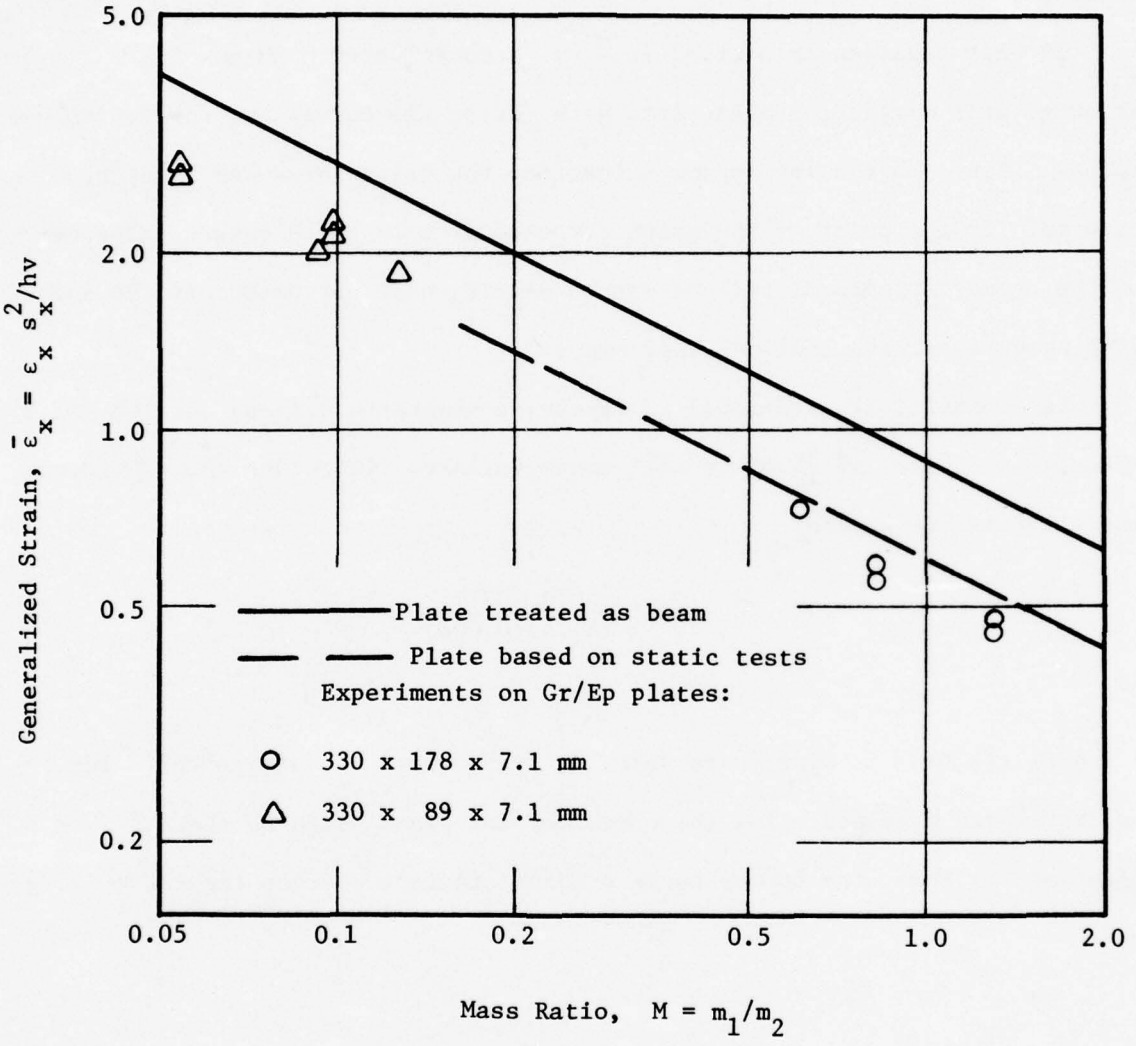

Figure 13. Design Curves and Experimental Data for Cantilever Plates

SECTION III

LOCAL RESPONSE BY A FINITE-DIFFERENCE METHOD

1. The ANEL Code

The ANEL code is essentially a modified version of the HEMP code, with the addition of anisotropic elastic constitutive relation, and plane stress problem capability.

The HEMP code was originally developed by Mark L. Wilkins [4] of Lawrence Radiation Laboratory, Livermore, California. The code has been used successfully to handle problems involving elastic, plastic, and/or hydrodynamic constitutive equations. In [4], example calculations included the problem of the detonation of an explosive charge against a copper plate and the detonation of an explosive charge in an iron cylinder. Karpp[10] has also used HEMP successfully for such classical problems as the expansion of an idea gas under high pressure in a tube, the impact of two identical blocks, and the problem of a cylindrical explosive charge accelerating an aluminum disc.

HEMP is described as a two dimensional finite difference "Lagrangian" code since it traces the position of the material particle. In the elastic range the material is assumed to follow the isotropic Hooke's law, and in the plastic range it is assumed to obey von Mises' yield condition. Two general classes of problems can be solved by the code, the plane strain problem and the axisymmetrical type of problem where the x axis is taken as the axis of symmetry. The code itself is well documented by E.D. Giroux [11].

The modification of HEMP involved the replacement of the isotropic Hooke's law by a generalized linear anisotropic constitututive equation. The equation of state was replaced by the anisotropic elastic relation

$$\dot{\sigma}_m = \frac{1}{3} [C_{iik\ell}\, \dot{e}_{k\ell} + C_{iikk}\, \dot{\varepsilon}_m]$$

which is an equation relating the spherical component of stress, σ_m, to the

mean strain, ε_m. In order to give HEMP the ability to handle anisotropic plane stress problems, some changes to the strain displacement relations had to be effected. With these modifications, the new code ANEL can handle any type of anisotropic linearly elastic material and hence any type of composite layup for the plane strain and plane stress cases. Because of the inherent nature of the axisymmetrical type of problem, this aspect of the code is limited to material symmetries of no greater complexity than transversely isotropic.

In the next section the governing equations used in ANEL will be presented. Also a brief description of some of the finite difference techniques will be given. The remainder of the chapter will deal with the various test and sample calculations made with ANEL.

2. Governing Equations and Numerical Scheme

The ANEL code is basically the HEMP code with modified anisotropic elastic constitutive equations. In addition, we have also added in the ANEL code the capability of treating plane stress problems.

The formulation of the equations and the numerical scheme used in the HEMP code have been presented by Wilkins [4] and Karpp [10]. Wilkins' code and presentation are for the one-dimensional problem (uniaxial strain), the plane strain problem, and the axisymmetrical problem. Karpp's presentation of the governing equations is in Cartesian coordinates only. For clarity and continuity, we shall present all the governing equations and numerical scheme of ANEL independently; although many of the equations are identical to HEMP.

All the governing equations used are written with respect to a coordinate system fixed in space, which will be called the space coordinates. All vector and tensor quantities in the governing equations are written with components in these space coordinates. ANEL may be called a Lagrangian code because the properties and positions of the mass particles are traced in time. However, the position, velocity, stress and strain of these particles are all written with respect to the space coordinates. In this sense the code is Eulerian in nature. A better description would be to call the code a hybrid Eulerian-Lagrangian code.

The conservation of momentum equations used are

$$\rho \frac{D^2 x_1}{Dt^2} = \sigma_{1j,j} + \gamma(2-\gamma) \frac{\sigma_{12}}{x_2} \tag{41}$$

$$\rho \frac{D^2 x_2}{Dt^2} = \sigma_{2j,j} + \gamma(2-\gamma) \frac{(\sigma_{22} - \sigma_{33})}{x_2} \tag{42}$$

Here the index j takes on the values 1,2; comma j represents differentiation with respect to the coordinate x_j. The material derivative taken along a particle path is represented by D/Dt. For a plane stress or plane strain problem the space coordinates, x_1, x_2 would be the Cartesian coordinates x,y. For an axisymmetrical problem the space coordinates x_1, x_2 would be the cylindrical coordinates z and r. The position of the particle is given as x_1, x_2. The stress tensor is represented by σ_{ij} and the density by ρ. The tracer γ has the following definitions: $\gamma = 0$, plane strain problem; $\gamma = 1$, axisymmetrical problem; and $\gamma = 2$, plane stress problem.

The conservation of mass equation is given as

$$\frac{D\rho}{Dt} + \rho\, \dot{x}_{i,i} + \rho\gamma(2-\gamma)\, \frac{\dot{x}_2}{x_2} + \rho\, \frac{\gamma(\gamma-1)}{2}\, A\, \dot{x}_{1,1} + \rho\, \frac{\gamma(\gamma-1)}{2}\, B\, \dot{x}_{2,2} + \rho\, \frac{\gamma(\gamma-1)}{4}\, C(\dot{x}_{2,1} + \dot{x}_{1,2}) = 0 \tag{43}$$

Here the index i takes values of 1,2; $\dot{x}_1$ and $\dot{x}_2$ are the velocities of the particle in the x_1 and x_2 directions, respectively. The last three terms are needed only for the plane stress case and are discussed in Appendix C.

The strain rate $\dot{\varepsilon}$ is related to the particle velocity by the equations:

$$\dot{\varepsilon}_{ij} = \frac{1}{2}(\dot{x}_{i,j} + \dot{x}_{j,i}) \qquad i,j = 1,2 \tag{44}$$

$$\dot{\varepsilon}_{33} = \gamma(2-\gamma)\, \frac{\dot{x}_2}{x_2} + \frac{\gamma(\gamma-1)}{2}\, A\, \dot{x}_{1,1} + \frac{\gamma(\gamma-1)}{2}\, B\, \dot{x}_{2,2} + \frac{\gamma(\gamma-1)}{4}\, C(\dot{x}_{2,1} + \dot{x}_{1,2}) \tag{45}$$

$$\dot{\varepsilon}_{13} = \frac{\gamma(\gamma-1)}{2}\, D\, \dot{x}_{1,1} + \frac{\gamma(\gamma-1)}{2}\, E\, \dot{x}_{2,2} + \frac{\gamma(\gamma-1)}{4}\, F(\dot{x}_{2,1} + \dot{x}_{1,2}) \tag{46}$$

$$\dot{\varepsilon}_{23} = \frac{\gamma(\gamma-1)}{2} G \dot{x}_{1,1} + \frac{\gamma(\gamma-1)}{2} R \dot{x}_{2,2} + \frac{\gamma(\gamma-1)}{4} T(\dot{x}_{2,1} + \dot{x}_{1,2}) \tag{47}$$

Once again the coefficients A,B,C,D,E,F,G,R, and T are needed only for the plane stress case and will be discussed in Appendix C.

The strain rate deviator, $\dot{e}$ is, as usual, defined by

$$\dot{e}_{ij} = \dot{\varepsilon}_{ij} - \delta_{ij} \dot{\varepsilon}_m \qquad i,j = 1,2,3 \tag{48}$$

where the scalar $\dot{\varepsilon}_m$ is given by

$$\dot{\varepsilon}_m = \frac{1}{3} \dot{\varepsilon}_{qq} \qquad q = 1,2,3 \tag{49}$$

and δ_{ij} is the "Kronekar Delta" ($\delta_{ij} = 1$ if $i = j$ and $\delta_{ij} = 0$ if $i \neq j$).

The stress deviator S is

$$S_{ij} = \sigma_{ij} - \delta_{ij} \sigma_m \qquad i,j = 1,2,3 \tag{50}$$

where the scalar σ_m is given by

$$\sigma_m = \frac{1}{3} \sigma_{qq} \qquad q = 1,2,3 \tag{51}$$

The constitutive relationships are written in terms of the stress deviator, S; the spherical component of stress, σ_m, the strain rate deviator, e; the mean strain rate, $\dot{\varepsilon}_m$; and the stiffness constants, $C_{ijk\ell}$.

$$\frac{\mathcal{D}s_{ij}}{\mathcal{D}t} = \frac{1}{3} [3C_{ijk\ell} - C_{qqk\ell} \delta_{ij}]\dot{e}_{k\ell} + \frac{1}{3} [3C_{ijkk} - C_{qqkk} \delta_{ij}]\dot{\varepsilon}_m \tag{52}$$

$$\frac{D \sigma_m}{Dt} = \frac{1}{3} [C_{iik\ell} \dot{e}_{k\ell} + C_{iik\ell} \dot{\varepsilon}_m] \tag{53}$$

where $C_{ijk\ell}$ is the general stiffness matrix of the anisotropic elastic medium.

The derivation of these two equations from the generalized Hooke's law

$$\sigma_{ij} = C_{ijk\ell}\ \varepsilon_{k\ell}$$

is given in Appendix D. Equations 52 and 53 represent three-dimensional equations, and the indices run over 1,2, and 3. The time derivative operating on the stress deviator tensor in Eq.(52) is the Jaumann [12] derivative. This derivative gives not only the variation of a tensor with respect to time, but also the variation of the tensor due to the rotation of the coordinate system to which it is referred.

Equations (41)-(53) constitute 29 independent equations ((52) and (53) are equivalent to 6 independent equations), in the 29 variables: σ_{ij}, S_{ij}, σ_m, $\dot{\varepsilon}_{ij}$, $\dot{e}_{ij}$, $\dot{\varepsilon}_m$, ρ, x_1,x_2. Now a short description of the finite difference scheme used in ANEL will be presented.

The governing equations are integrated by a finite difference technique. The material is initially divided into grid zones by a rectangular mesh. The sides of the grid zones are initially parallel to the fixed space coordinate system x_1, x_2. Each grid zone always encompasses a fixed amount of mass and will move with this mass as it translates, distorts, dilates, and rotates. In other words the grid zone is fixed in the material. Tensors such as $\dot{\varepsilon}$, $\dot{e}$, σ, S and scalars such as ρ, $\dot{\varepsilon}_m$, and σ_m are calculated as the average over the grid zone area. Vectors such as x_1, x_2, the particle position and particle velocity $\dot{x}_1$, $\dot{x}_2$ are referred to the grid zone corners.

The material derivative D/Dt is approximated in finite difference form as

$$\frac{D}{Dt} f_0 \sim \frac{f_0(t+\Delta t) - f_0(t)}{\Delta t} \qquad (54)$$

where f_0 is either a scalar or a vector fixed to the moving particle. The

difference in f_0 is taken between two successive times that are separated by the time increment Δt.

The Jaumann derivative which is used in Equation (52) operates on the stress tensor. In finite difference form it is approximated by

$$\frac{\mathcal{D}S_{ij}}{\mathcal{D}t} \sim \frac{1}{\Delta t} \left[S_{ij}\ (t+\Delta t) - S_{ij}(t) \right] \tag{55}$$

The stress states in Equation (55) are written with their components in the space coordinates. The stress components calculated at time t have rotated an angle ω_{21} during the time Δt, and this shall be designated as $S'_{ij}(t)$. In Equation (55) $S_{ij}(t)$ are the projections of $S'_{ij}(t)$ on the space coordinates, or

$$S_{ij}(t) = a_{ik}\ a_{j\ell}\ S'_{k\ell}(t) \tag{56}$$

where

$$a_{ij} = \begin{bmatrix} \cos(-\omega_{21}) & -\sin(-\omega_{21}) & 0 \\ \sin(-\omega_{21}) & \cos(-\omega_{21}) & 0 \\ 0 & 0 & 1 \end{bmatrix} \tag{57}$$

and

$$\omega_{21} = \Delta t\ \dot{\omega}_{21} = \frac{\Delta t}{2} \left(\frac{\partial \dot{x}_2}{\partial x_1} - \frac{\partial \dot{x}_1}{\partial x_2} \right) \tag{58}$$

For small deformation, the difference between $S'_{ij}(t)$ and $S_{ij}(t)$ is negligible.

The partial space derivatives are obtained by the use of Green's Theorem and the Mean Value Theorem. For example to find $\frac{\partial f}{\partial x_1}$ we use Green's Theorem which states that

$$\int\int_R \frac{\partial f}{\partial x_1}\, dx_1\, dx_2 = \oint_C f\, dx_2 \tag{59}$$

in conjunction with the Mean Value Theorem stating

$$\frac{\partial f}{\partial x_1} \oint_C x_1 \, dx_2 = \int\int_R \frac{\partial f}{\partial x_1} \, dx_1 \, dx_2 \tag{60}$$

Combining these two, we get

$$\frac{\partial f}{\partial x_1} = \frac{\oint_C f \, dx_2}{\oint_C x_1 dx_2} = \frac{\oint_C f \, dx_2}{A} \tag{61}$$

where A is the area of the region R enclosed by the contour C. Likewise

$$\frac{\partial f}{\partial x_2} = \frac{-\oint_C f \, dx_1}{A} \tag{62}$$

These two equations for the partial space derivatives are approximated as

$$\left.\frac{\partial f}{\partial x_1}\right|_0 \sim \frac{1}{A}\left\{f_a\,[x_2(1) - x_2(4)] + f_b[x_2(2) - x_2(1)] + f_c\,[x_2(3) - x_2(2)] + f_d[x_2(4) - x_2(3)]\right\} \tag{63}$$

$$\left.\frac{\partial f}{\partial x_2}\right|_0 \sim -\frac{1}{A}\left\{f_a\,[x_1(1) - x_1(4)] + f_b[x_1(2) - x_1(1)] + f_c\,[x_1(3) - x_1(2)] + f_d[x_1(4) - x_1(3)]\right\} \tag{64}$$

where the numbers in parenthesis designate the grid points 1,2,3, and 4 shown in Figure 1 and the subscripts on f represent the average values of f over the grid zone areas a,b,c, and d.

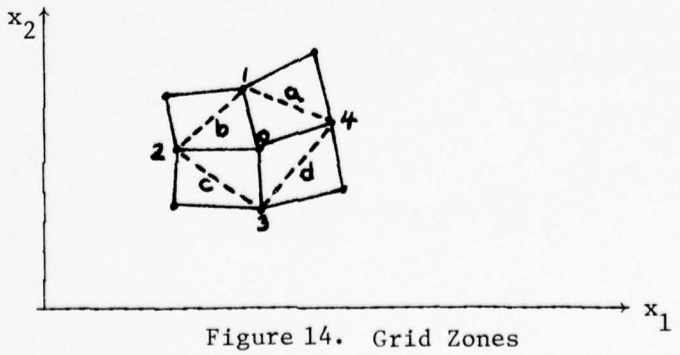

Figure 14. Grid Zones

The area A is the area of the dotted quadrilateral.

As mentioned before when describing the constitutive equation 52 the stiffness constants must be written with components in the space coordinates x_1, x_2. The material stiffness constants $C'_{ijk\ell}$ are referred to a material coordinate system X_1, X_2 fixed in the material.

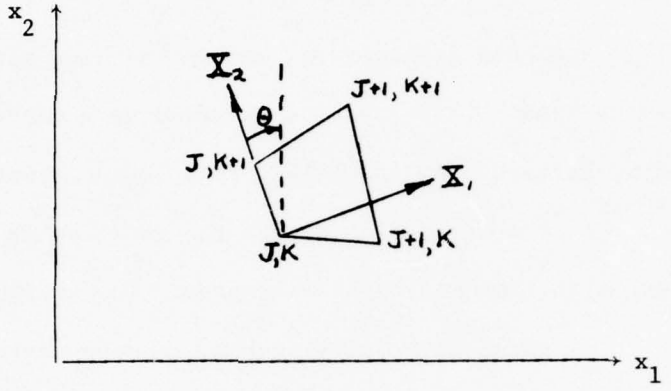

Figure 15. Material Coordinates X_1 X_2

Since an originally rectangular material grid may not stay rectangular, the "material coordinates" are not always automatically defined. We have arbitrarily assigned the X_2 axis to be fixed with one side of the material grid connecting points (J,k) and (J,k+1); as a result, the X_1 axis which is orthogonal to X_2 is not necessarily along the side of the grid connecting (J,k) and (J+1,k) (See Figure 2). The angle between the X_2 axis and the vertical is given by

$$\theta = \tan^{-1} \left\{ \frac{x_1(J,k+1) - x_1(J,k)}{x_2(J,k+1) - x_2(J,k)} \right\} \tag{65}$$

The stiffness constants can be written with components in the space coordinate system by the transformation

$$C_{ijk\ell} = A_{mi} A_{pj} A_{qk} A_{r\ell} C'_{mpqr} \tag{66}$$

where the direction cosines A_{ij} are given by

$$A_{ij} = \begin{bmatrix} \cos\theta & -\sin\theta & 0 \\ \sin\theta & \cos\theta & 0 \\ 0 & 0 & 1 \end{bmatrix} \tag{67}$$

In the HEMP code only the strain rate tensor is calculated; strain is never defined. The strain increment $d\varepsilon_{ij}$ is referred to the current dimension and can be called the natural strain increment. In ANEL the strain has been calculated by the use of the following finite difference approximation.

$$\varepsilon_{ij}(t+\Delta t) = \dot{\varepsilon}_{ij}\left(t+\frac{\Delta t}{2}\right)\Delta t + \varepsilon_{ij}(t) \tag{68}$$

Here the mass particle has been followed and strain has been obtained by integrating step-by-step in time. This may be considered as a material time integral as defined by Malvern [13] (p. 151). This strian, however, is clearly an approximation because no contribution due to the rotation of the mass particle as it advances in time has been considered. The strain rate is always referred to the space coordinate system. A more correct way to get the strain would be to treat it the same way as was done with the stress tensor by taking into account the rotation of the mass particle. In short the values of strain that have been calculated in ANEL may be considered as Lagrangian with respect to translation but Eulerian with respect to rotation.

The set of algebraic finite-difference equations are used to calculate from the known quantities at time t the solution of the unknowns at time $t+\Delta t$. Figure 16 gives a flow chart of the order in which the governing equations (in finite difference form) are used. Note that we begin with the stress state σ_{ij}, the density ρ, and the particle position x_1, x_2 known at $t = t$. Eqs.(41)-(42) are used to obtain the particle velocity half way between the two time planes or $t = t + \frac{\Delta t}{2}$. Here we have really integrated Eqs.(41)-(42) once in time to get $\frac{Dx_i}{Dt}$ (also written as $\dot{x}_1$, $\dot{x}_2$). By using the following finite difference equation the particle position at $t = t + \Delta t$ is obtained

$$x_i(t+\Delta t) = \dot{x}_i(t+\tfrac{\Delta t}{2})\Delta t + x_i(t)$$

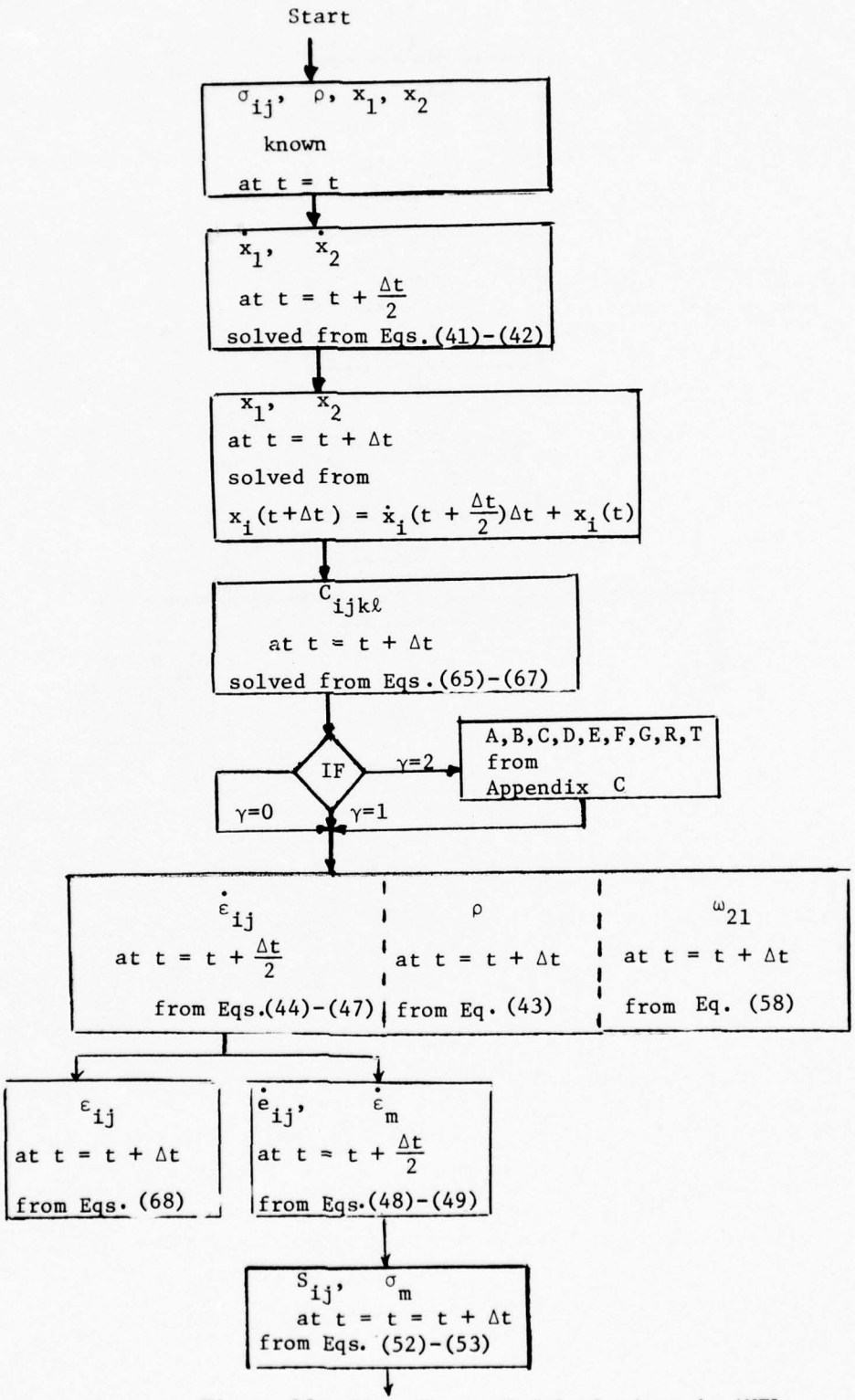

Figure 16. Flow Chart of Calculations in ANEL

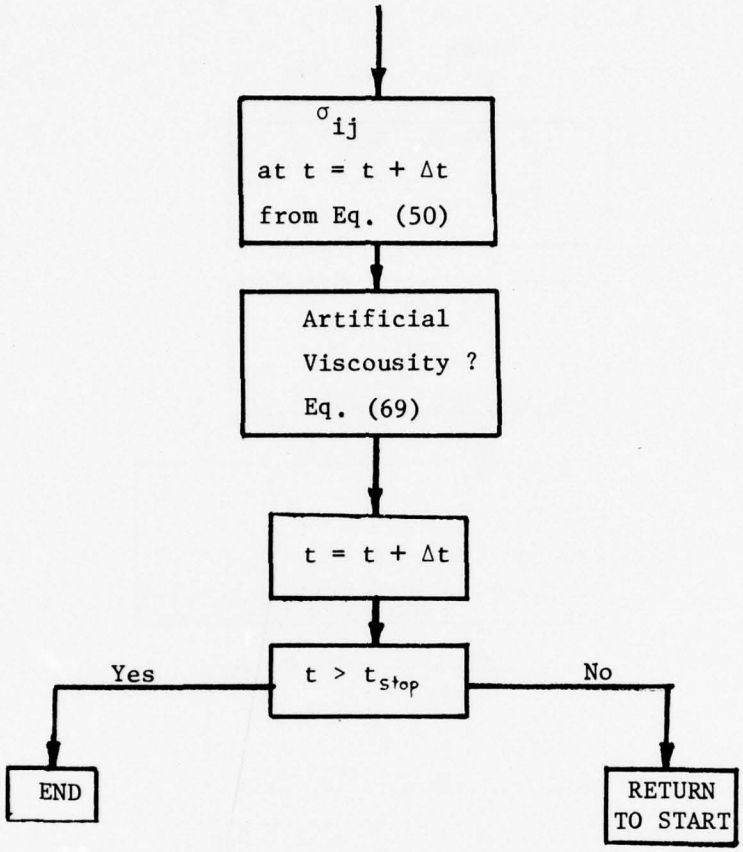

Figure 16. Flow Chart of Calculations in ANEL (Cont.)

Now using Eqs. (65)-(67) the stiffness constants $C_{ijk\ell}$ are obtained. Next the type of problem considered is decided: plane strain, $\gamma = 0$; axisymmetric, $\gamma = 1$; and plane stress, $\gamma = 2$. Note only for the case $\gamma = 2$, will the coefficients A,B,C,D,E,F,G,R, and T be calculated as described in Appendix C. The next group of steps produce the density ρ at $t+\Delta t$ by use of Equation (43), the strain rate tensor $\dot{\varepsilon}_{ij}$ at $t+\frac{\Delta t}{2}$ from Eqs.(44)-(47), and the angle of rotation ω_{21} at $t+\Delta t$ from Equation (58). Now knowing $\dot{\varepsilon}_{ij}$, Eqs.(48)-(49) are used to give $\dot{e}_{ij}$ and $\dot{\varepsilon}_m$ at time $t + \frac{\Delta t}{2}$. As is indicated in Figure 16 the strain tensor ε_{ij} at time $t+\Delta t$ is calculated by Eqs. (68). S_{ij} and σ_m are obtained at time $t+\Delta t$ by using the constitutive equations Eqs. (52)-(53). Equation (50) now gives σ_{ij} at time $t+\Delta t$. The artificial viscousity is calculated as

$$q = \frac{C\rho_0 A}{v}\left[\frac{\dot{v}}{v}\right]^2 \quad \text{if} \quad \frac{\dot{v}}{v} < 0 \tag{69}$$

$$q = 0 \quad \text{if} \quad \frac{\dot{v}}{v} \geq 0$$

where

$$v = \frac{1}{\rho}$$

$$\frac{\dot{v}}{v} = -\frac{\dot{\rho}}{\rho}$$

C = a constant

A = grid zone area.

This term is subtracted from σ_{11} and σ_{22} and σ_m. The purpose of this term is to smooth out the effect of a shock wave over several grid zones and is based upon the von Neumann-Richtmyer method. The time is now incremented by Δt and if this new time is not greater than the stopping time, t_{stop} the program repeats the process. It should be noted that the time increment Δt is an inputted constant in ANEL.

In the next section several runs and comparisons using ANEL are discussed.

3. An Axisymmetrical Impact Problem

As a partial check of the code, a problem with isotropic material was solved by ANEL and the results compared with those of HEMP. The problem involved an isotropic cylinder subjected to a point load along its axis of symmetry. The cylinder had a length of 4 cm and a radius of 4 cm. Young's modulus used was E = 2.07 Mbar and the shear modulus was G = .796 Mbar. The density of the body was $\rho = 7.8$ gm/cm^3. The point load of 2.62×10^8 dynes was applied gradually in time and then held constant. Furthermore, in order to avoid any instability in either program due to the discontinuous nature of a point load, the force was replaced by a conical pressure distribution. The form of this pressure distribution in time t and radius r is

$$P = P_0\left[1 - \frac{r}{a}\right]\left\{\frac{2t}{t_0} - \left(\frac{t}{t_0}\right)^2\right\} \qquad \begin{matrix} t < t_0 \\ r < a \end{matrix}$$

$$P = P_0\left[1 - \frac{r}{a}\right] \qquad \begin{matrix} t \geq t_0 \\ r < a \end{matrix}$$

$$P = 0 \qquad r \geq a$$

where a = 0.5 cm, t_0 = 1 μsec, and P_0 = 0.001 Mbar*

Both programs were run as axisymmetrical cases. The mesh size used in the region closest to the axis of symmetry was 1x3 mm and the constant time step used throughout the calculations was $\Delta t = 0.02$ μsec.

Figure 17, shows a time history of the normal stress σ_{zz} at the location r = 1.02 cm, z = 2.12 cm. The curve plotted is the same for both the HEMP run and the ANEL run. This indicates that ANEL can handle an isotropic elastic problem and gives very favorable results when compared with HEMP.

Another problem was solved by ANEL and the results compared with an existing numerical solution. The problem consisted of a semi-infinite composite subjected to an impact of a rigid sphere. In Ref. [14], Greszczuk solved

* ANEL uses the c.g. μsec system of units: length - cm, mass - g, time - μsec, force - 10^{12} dynes, and pressure - Mbar.

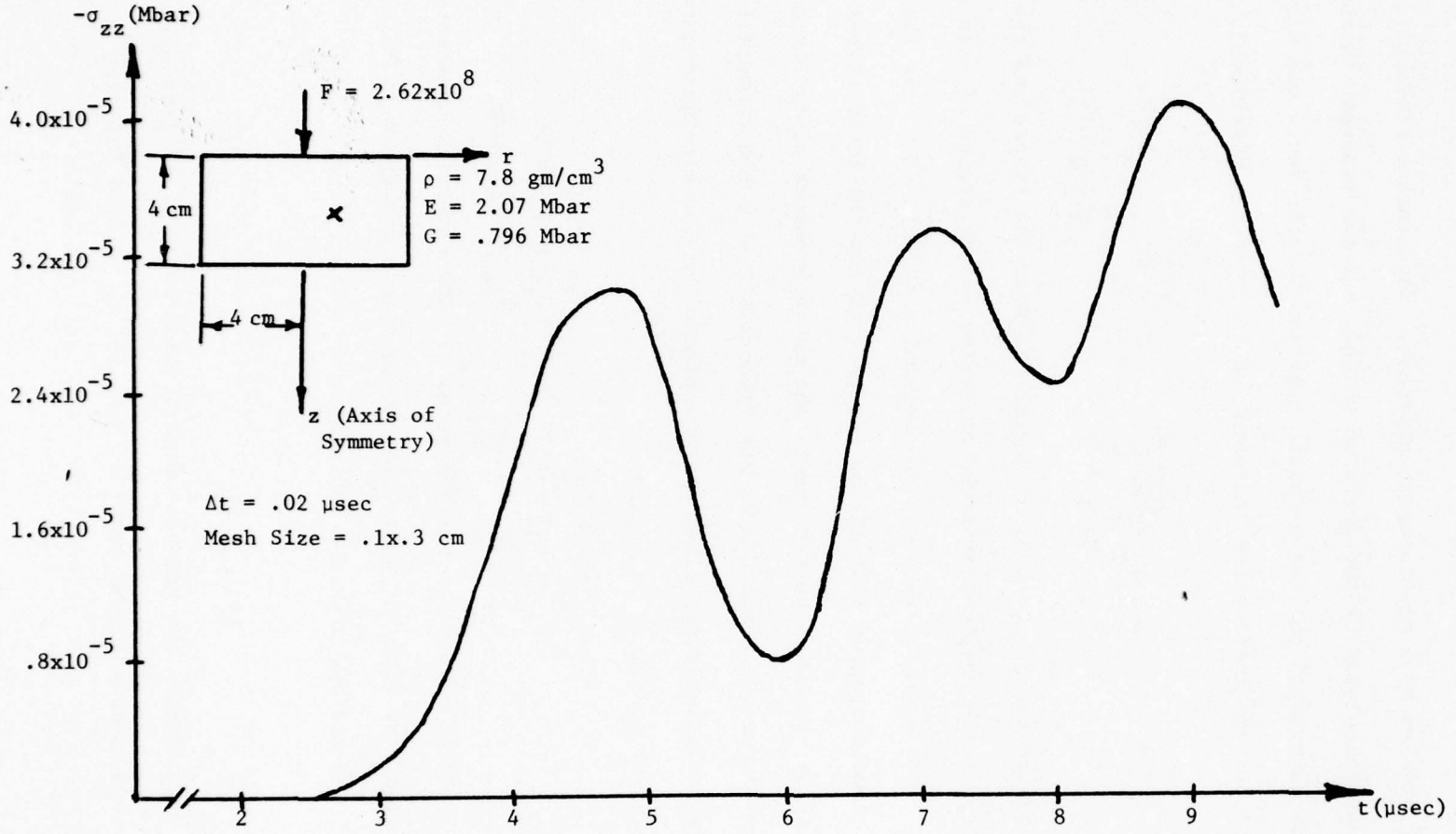

Figure 17. Comparison Between the Isotropic HEMP and the Anisotropic ANEL Codes for the Problem of a Concentrated Load F Suddenly Applied on an Isotropic Body. Curve shows Stress σ_{zz} at r = 1.02 cm, z = 2.12 cm for both Codes.

this impact problem by a quasi-static approach. The contact pressure distribution was calculated by the Hertzian method, but the response in the composite is calculated only as a static problem, inertia force was neglected. He assumed a surface indentation and obtained the pressure distribution of the form

$$P = q_0 \sqrt{1 - \frac{r}{a}} \qquad r < a$$

$$P = 0 \qquad r \geq 0$$

where a is the radius of the area of contact between the sphere and the target surface and q_0 is the maximum pressure occurring at the center of this area of contact. This approach is shown schematically in Fig. 18. By the use of the finite element program SAAS III he was able to get the local stress distribution in the composite target due to the above pressure distribution.

For the comparison between ANEL and Greszczuk's work the composite chosen was a transversely isotropic glass epoxy laminate. The elastic constants used in c.g. μsec system of units are

$$E_{zz} = 0.2 \text{ Mbar} \qquad \nu_{r\theta} = 0.32$$

$$E_{rr} = E_{\theta\theta} = 0.305 \text{ Mbar} \qquad G_{zr} = G_{z\theta} = 0.06 \text{ Mbar}$$

$$\nu_{zr} = \nu_{z\theta} = 0.091 \qquad G_{r\theta} = 0.115 \text{ Mbar}$$

The density used in ANEL was $\rho = 1.995 \text{ gm/cm}^3$. The stiffness constants $C_{ijk\ell}$ as calculated from the above elastic constants are given in Table 7.

In [14] the maximum pressure and radius of contact were

$$q_0 = 0.00031 \text{ Mbar}$$

$$a = 0.5 \text{ cm}$$

In the ANEL calculation the pressure distribution was applied gradually in time and then held constant as shown in Fig. 19. A true Hertzian pressure

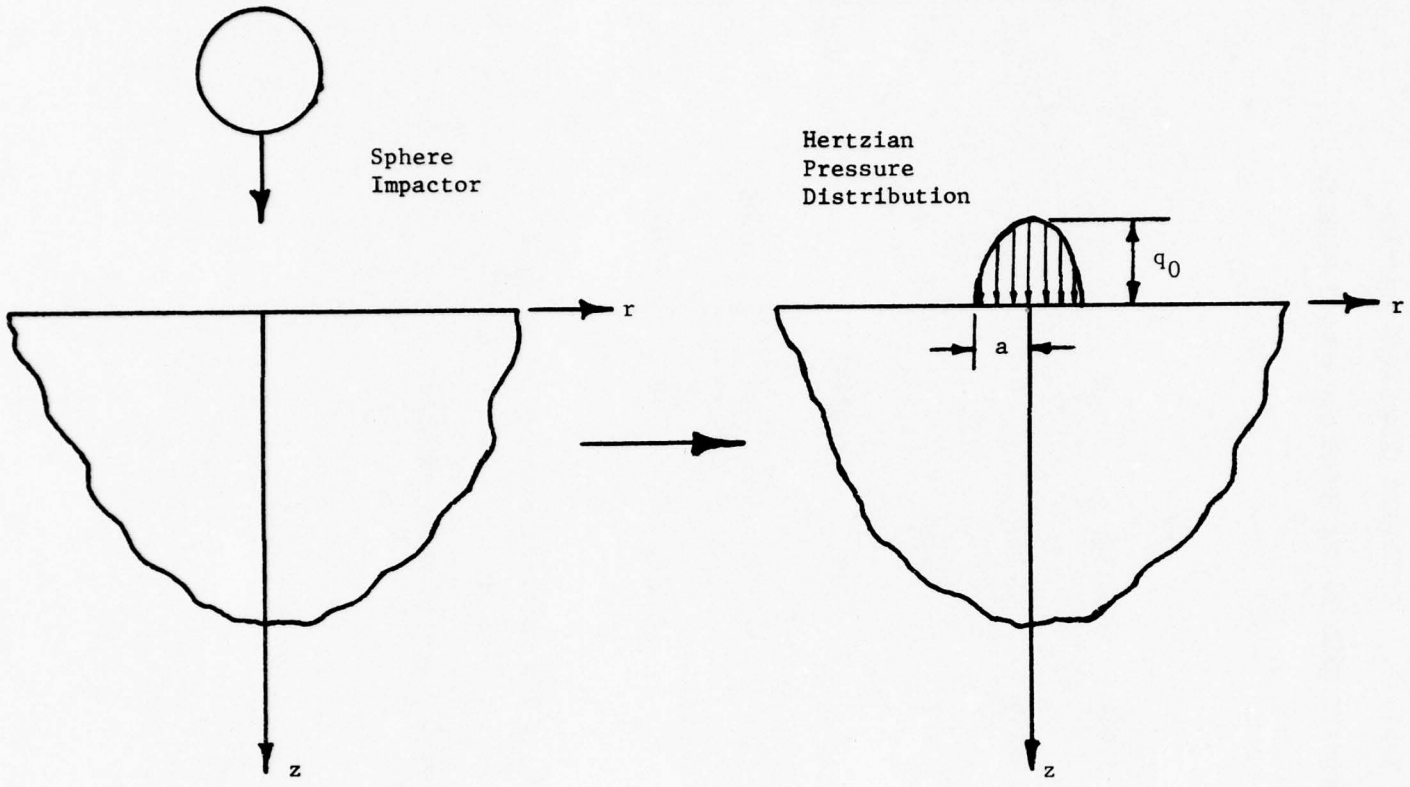

Figure 18. Impact of a Sphere on a Semi-Infinite Anisotropic Medium

Table 7. STIFFNESS CONSTANTS FOR THE COMPOSITE USED IN THE HERTZIAN IMPACT PROBLEM

$$C_{ij} = \begin{bmatrix} 0.208 & 0.042 & 0.042 & 0 & 0 & 0 \\ 0.042 & 0.348 & 0.117 & 0 & 0 & 0 \\ 0.042 & 0.117 & 0.348 & 0 & 0 & 0 \\ 0 & 0 & 0 & 0.115 & 0 & 0 \\ 0 & 0 & 0 & 0 & 0.06 & 0 \\ 0 & 0 & 0 & 0 & 0 & 0.06 \end{bmatrix}$$

Notes 1) $C_{ijk\ell} = C_{qr}$, The contraction notation is used

2) Values of C_{ij} are in units of Mbar.

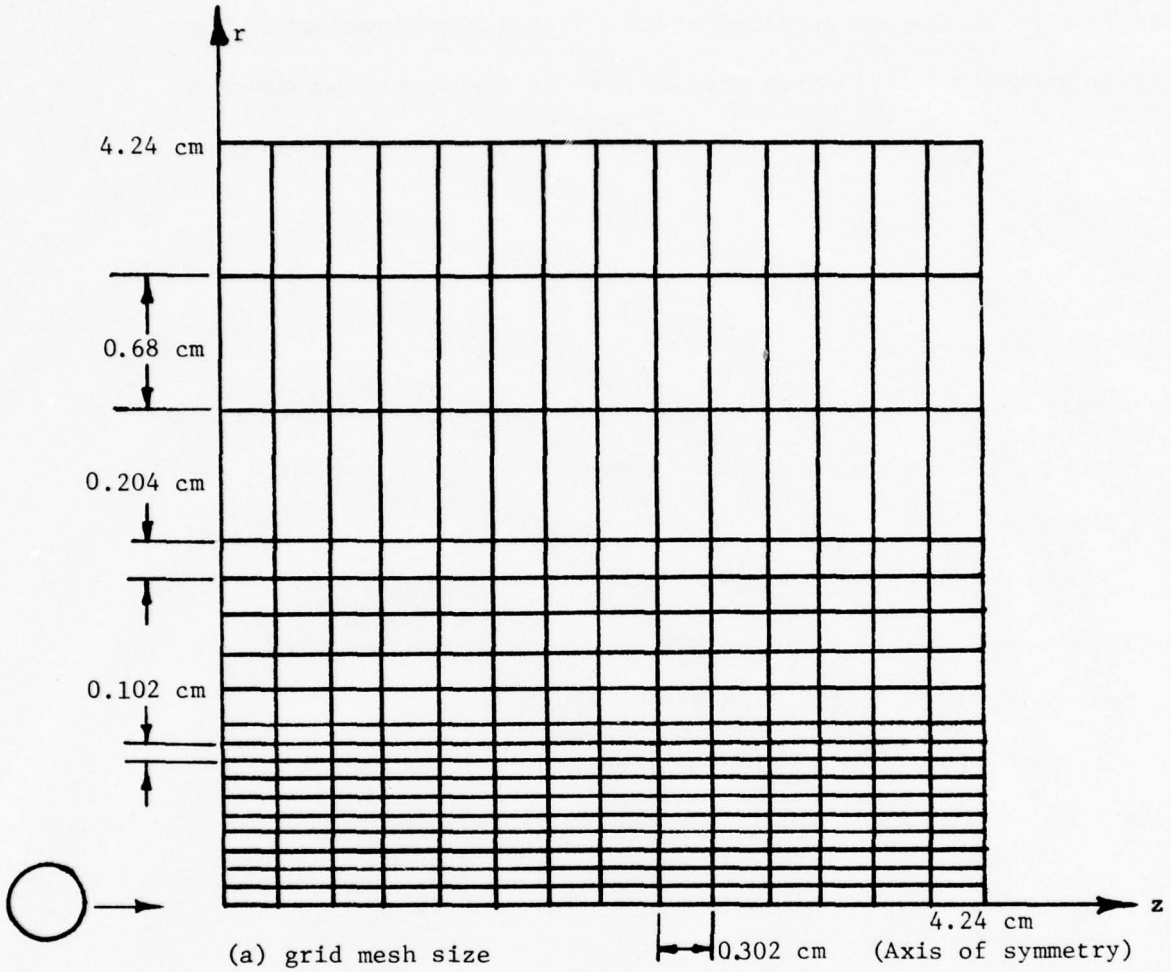

(a) grid mesh size

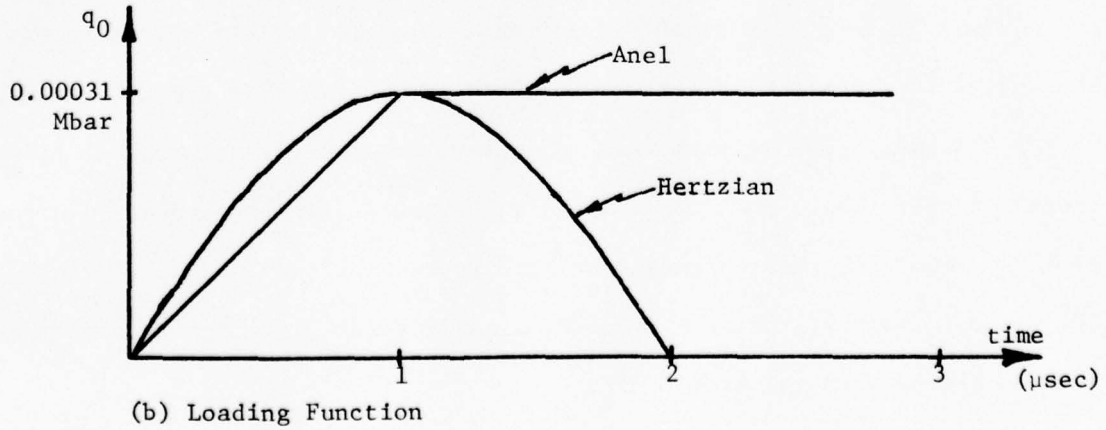

(b) Loading Function

Figure 19. Glass Epoxy Under Impact of Rigid Sphere

distribution in time is included on this figure for comparison. The loading pressure distribution used in ANEL is now summarized below as

$$P = q_0 \sqrt{1 - \frac{r}{a}} \; \frac{t}{t_0} \qquad \begin{matrix} r < a \\ t < t_0 \end{matrix}$$

$$P = q_0 \sqrt{1 - \frac{r}{a}} \qquad \begin{matrix} r < a \\ t \geq t_0 \end{matrix}$$

$$P = 0 \qquad r \geq a$$

where $t_0 = 1$ μsec.

The target was a cylinder of radius 4.24 cm and depth 4.24 cm. The grid zoning used is shown in Figure 19. The constant time step used was $\Delta t = 0.02$ μsec.

Figure 20 gives a time history of the normal stress σ_z/q_0 at a location on the axis of symmetry 0.9 cm away from the center of impact. The maximum value of normal stress occurs at $t = 4.4$ μsec.

Figure 21 is a plot of the axial distribution of normal stress. The solid line is from ANEL and was plotted for the time $t = 4.4$ μsec. The dashed line is the static, finite element solution from [14]. Although both solutions start at the same value of stress, $\sigma_z/q_0 = 1$ at $z/a = 0$, the dynamic solution is higher at all other points than the static solution.

Figure 22 is a plot of the radial distribution of shear stress along the radial line $z/a = 0.6$. The solid curve is plotted from the ANEL solution at $t = 2.4$ μsec. The maximum value of shear stress along this radial line occurs at this time. The dashed line is the static finite element solution of [14]. The peak shear stress from both approaches occurs approximately at $r/a = 0.8$. However, the peak from the dynamic solution is approximately fifty percent higher than the static solution.

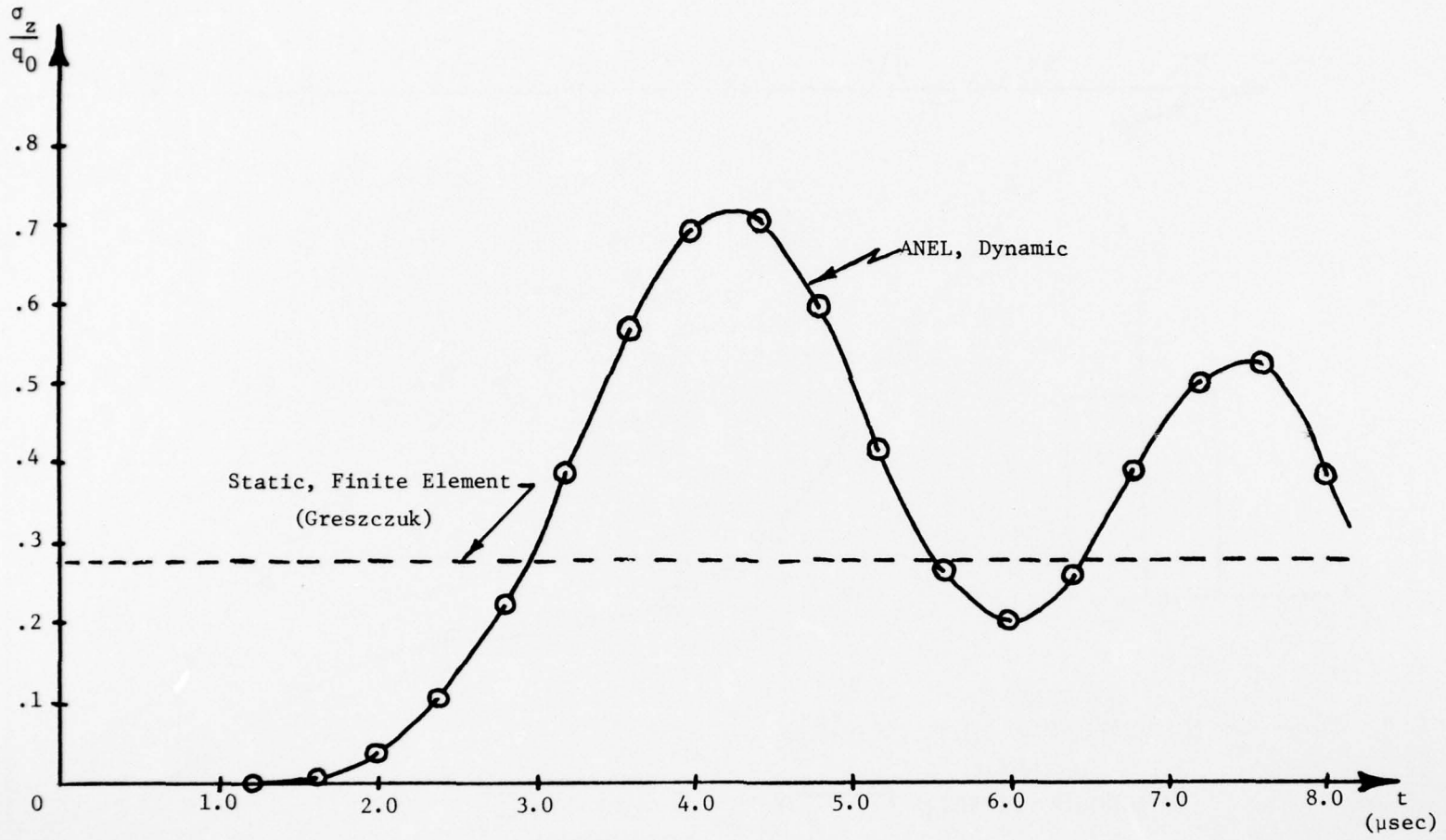

Figure 20. Time History of Normal Stress at $z/a = 1.8$, $r/a = 0$

Glass Epoxy Under Impact of Rigid Sphere

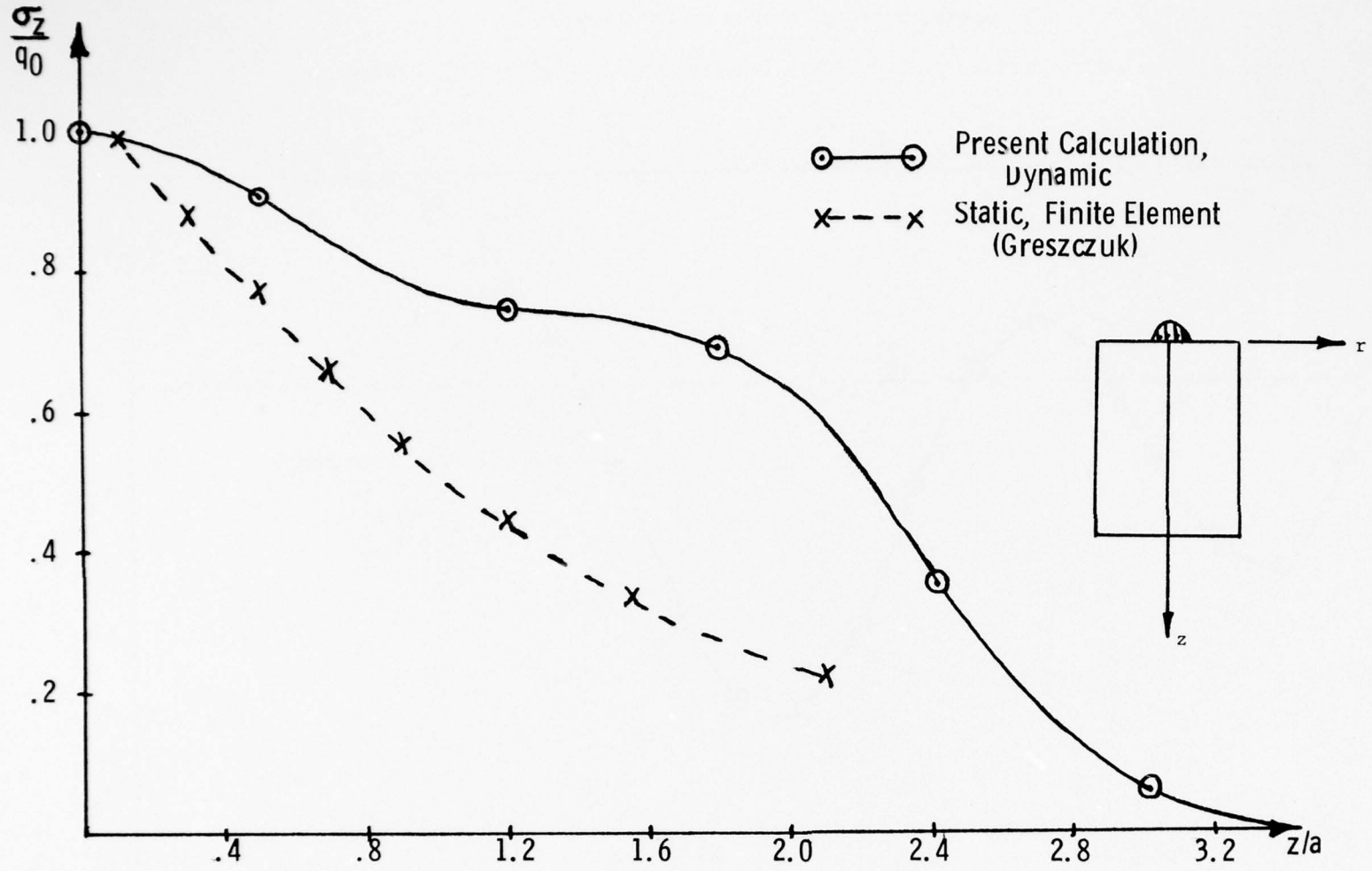

Figure 21. Axial Distribution of Normal Stress at 4.4 μsec. (r=0)
Glass Epoxy Under Impact of Rigid Sphere

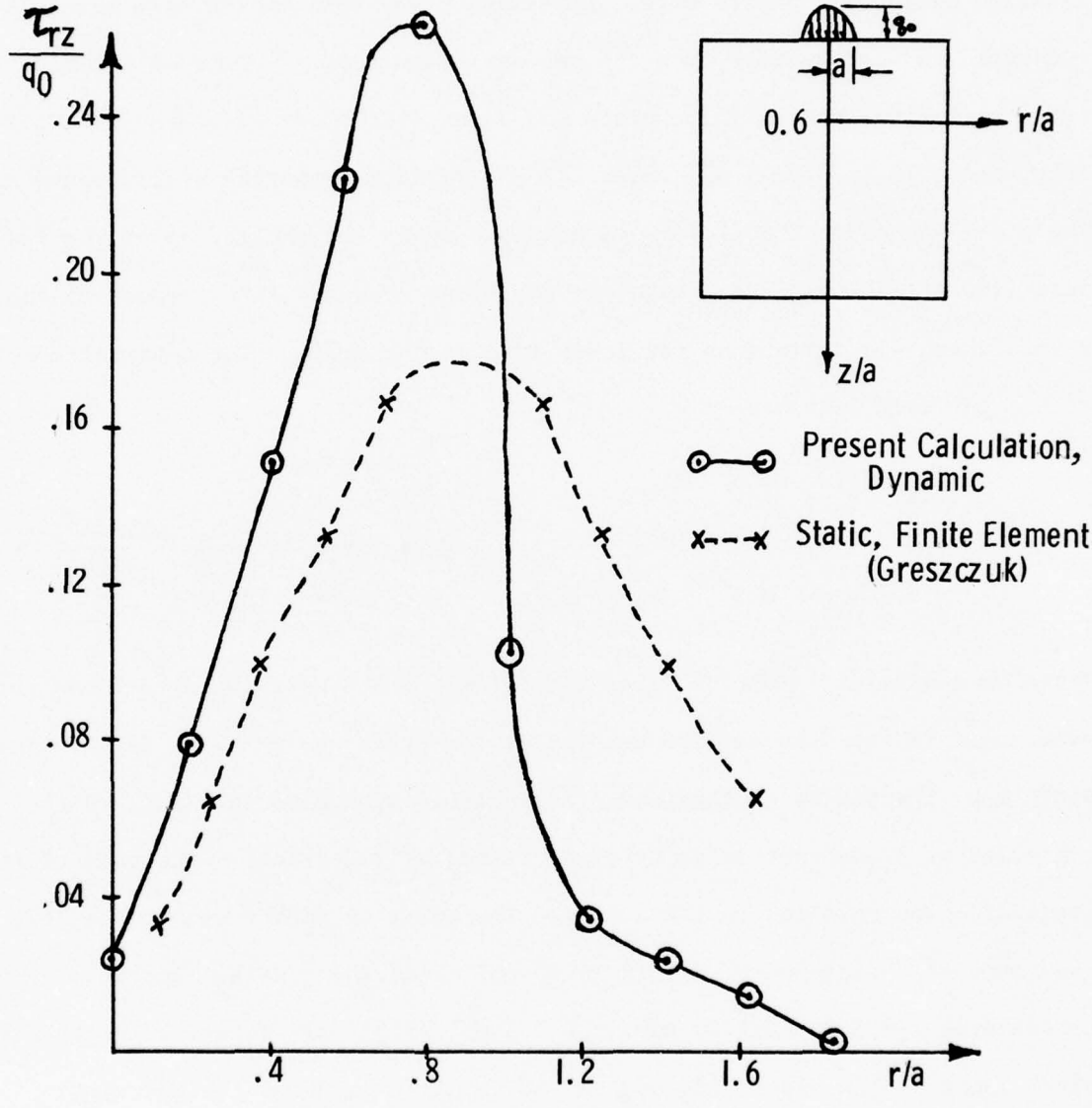

Figure 22. Radial Distribution of Shear Stress at 2.4 μsec and z/a=0.6 Glass Epoxy Under Impact of Rigid Sphere

4. A Plate Edge Impact Problem

Another calculation was made of a cantilever plate impacted by an aluminum projectile on its edge. Experiments for this impact case were also conducted and the results from the two were compared. Figure 23 shows the experimental set up. The plate was 7 in. (17.78 cm) wide, 13 in. (33.02 cm) long, and 0.28 in. (0.71 cm) thick and was rigidly supported at its upper edge. The plate was made of 50 layers of graphite epoxy and the lay-up of the laminae were $((90,45,90,-45)_6,90)_S$ where the angle was measured with respect to the x-axis which was defined as the lower edge of the plate. The material constants for each lamina were

$$E_{11} = 17.7 \times 10^6 \text{ PSI} \qquad \nu_{23} = 0.2$$

$$E_{22} = E_{33} = 1.3 \times 10^6 \text{ PSI} \qquad G_{12} = G_{13} = 0.55 \times 10^6 \text{ PSI}$$

$$\nu_{12} = \nu_{13} = 0.3 \qquad G_{23} = 0.54 \times 10^6 \text{ PSI}$$

where the subscript 1 was the fiber direction and 2,3 were the directions perpendicular to the fibers. The density of the plate was $\rho = 1.51$ g/cm^3. The plate was impacted by an aluminum projectile of mass 0.06 lb (27 g) which travelled at a constant velocity of 40 ft/sec (12.2 m/sec). The path of the projectile was parallel to the x axis. The point of impact was on the left hand edge at a distance of 2.5 in (6.35 cm) above the x axis. At the coordinates x = 5 in. (12.70 cm), y = 2.5 in. (6.35 cm) two strain gages were placed, one on the upper side and one on the lower side of the plate, to monitor bending stress.

The conventional method of handling a composite plate problem is to use the lamination theory (see ref. [9]). The known values of the lamina engineering constants E's and ν's are first converted into plane stress

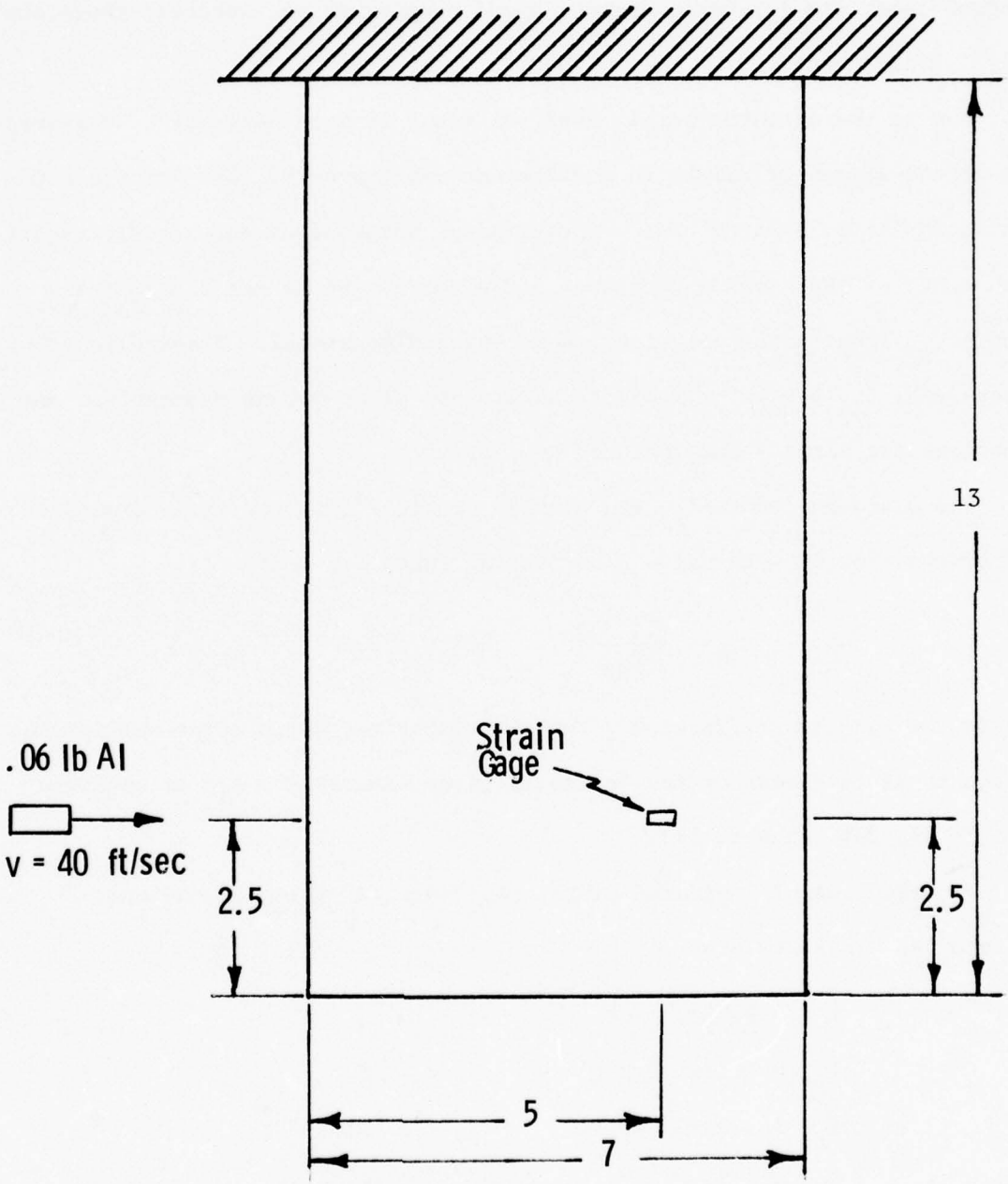

Figure 23. Graphite Epoxy Plate Subject to Edge Impact
All Dimensions in Inch

"reduced" stiffness constants Q_{ij}. These Q_{ij} are then transformed into the plate coordinates and summed to give the A_{ij}, B_{ij} and D_{ij} matrices. For the present case, the lay-up is symmetric and bending is not induced; therefore only A_{ij} are needed.

Due to the arrangements in HEMP, we found it more convenient to express the stress-strain relations in a different way for ANEL. The layered composite is first "smeared" into an equivalent homogeneous anisotropic material, with a set of engineering constants and a corresponding set of stiffness constants C_{ij} (contracted notation), both three-dimensional. These three-dimensional C_{ij} are to be fed into ANEL. The plane stress assumptions and equations are already incorporated in ANEL.

The plate constants A_{ij} can also be obtained from the three dimensional C_{ij} of the smeared material. Substituting these C_{ij} into

$$Q_{ij} = C_{ij} - \frac{C_{i3}\, C_{j3}}{C_{33}} \qquad i,j = 1,2,6$$

yields the reduced stiffness Q_{ij} for the composite, which after multiplying by the total thickness of the laminate, gives exactly the A_{ij} as obtained from Eq. (3-25) of Ref. [9].

For the present laminated plate, the "smeared" three-dimensional engineering constants are

$E_{xx} = 2.9 \times 10^6$ PSI
$E_{yy} = 10.3 \times 10^6$ PSI
$E_{zz} = 1.3 \times 10^6$ PSI
$\nu_{xy} = 0.20$
$\nu_{yz} = 0.15$
$\nu_{xz} = 0.18$
$G_{xy} = 2.5 \times 10^6$ PSI
$G_{yz} = 0.55 \times 10^6$ PSI
$G_{xz} = 0.54 \times 10^6$ PSI

The stiffness constants in Mbars for this equivalent medium are given in Table 8. The material symmetry of the equivalent medium is orthotropic.

In the numerical calculation, the plate is divided into square grids, each with sides of 0.47 in. (1.2 cm). The lower edge, left hand side edge, and the right hand side edge were specified as free boundaries. The upper edge was specified as a fixed boundary.

In order to model the impact loading the Hertzian method described by Goldsmith [15] was used. First the projectile was simulated by an aluminum ball with the same mass and a radius of 1.3 cm, and the same velocity as the original projectile. The pressure distribution according to Eqs. (4.13, 4.33) of [15] was then

$$P = P_m \sqrt{1 - \left(\frac{r}{a_m}\right)^2} \sin\left(\frac{\pi t}{t_0}\right) \qquad \begin{matrix} t \leq t_0 \\ r \leq a_m \end{matrix}$$

$$P = 0 \qquad \text{and/or} \qquad \begin{matrix} t \geq t_0 \\ r \geq a_m \end{matrix}$$

where $$P_m = \frac{3 F_m}{2\pi a_m^2}$$

and

a_m = the maximum radius of the area of contact = 0.21 cm

t_0 = the impact duration = 81 μsec

F_m = maximum impact force = $.0014 \times 10^{12}$ dynes .

Because of the large mesh size used, this pressure distribution covers less than one grid zone and was considered unsatisfactory; instead, a rectangular pressure distribution of the same duration in time with the same total force but larger contact area was used, and is given below as

Table 8. STIFFNESS CONSTANTS USED FOR LAMINATED GRAPHITE EPOXY PLATE

$$C_{ij} = \begin{bmatrix} 0.236 & 0.168 & 0.023 & 0 & 0 & 0 \\ 0.168 & 0.832 & 0.031 & 0 & 0 & 0 \\ 0.023 & 0.031 & 0.094 & 0 & 0 & 0 \\ 0 & 0 & 0 & 0.038 & 0 & 0 \\ 0 & 0 & 0 & 0 & 0.037 & 0 \\ 0 & 0 & 0 & 0 & 0 & 0.171 \end{bmatrix}$$

Notes: 1) $C_{ijk\ell} = C_{qr}$, The contracted notation is used.

2) Values of C_{ij} are in units of Mbar.

$$P = P_0 \sin\left(\frac{\pi t}{t_0}\right) \qquad t \leq t_0 \quad 4.7\text{cm} \leq y \leq 8.3\text{ cm}$$

$$P = 0 \qquad t > t_0 \text{ and/or } 4.7\text{cm} > y > 8.3\text{cm}$$

where $P_0 = 5.4 \times 10^{-4}$ Mbar. As can be seen this pressure distribution spreads over three grid zones.

Figure 24 shows the comparison between ANEL and experiment of the strain at the location of the strain gage at x = 5 in. (12.70 cm) and y = 2.5 in. (6.35 cm). Great care was taken in the experimental study to obtain identical traces for the gages located on the upper and lower sides of the plate. Any deviation between the two would indicate bending and hence the plane stress assumption would not be applicable. The dashed line in the figure represents the reading of strain from the strain gage. About ten experimental trials were run and a statistical study was done on the peak strains and their times of occurrence and also on the time that the strain curve crossed the time axis. The coefficient of variation (i.e. the standard deviation divided by the mean) for these readings was found to be no greater than 12% in all cases. This indicates good reproducibility of the experimental results. The solid curve represents the solution obtained by ANEL. As can be seen the analytical solution has the same shape as the experimental results and the times of the peaks and zero strain are in good agreement. However, the magnitude of the peak strains from ANEL are greater than those obtained from the strain gage readings. This difference is about 110% for the first peak occurring at 65 μsec and about 130% for the second peak occuring at 120 μsec.

There are several explanations for this large discrepancy in peak strain shown in Figure 24. First the loading function could be inaccurate because the projectile was modelled as a ball of radius 1.3 cm when in reality

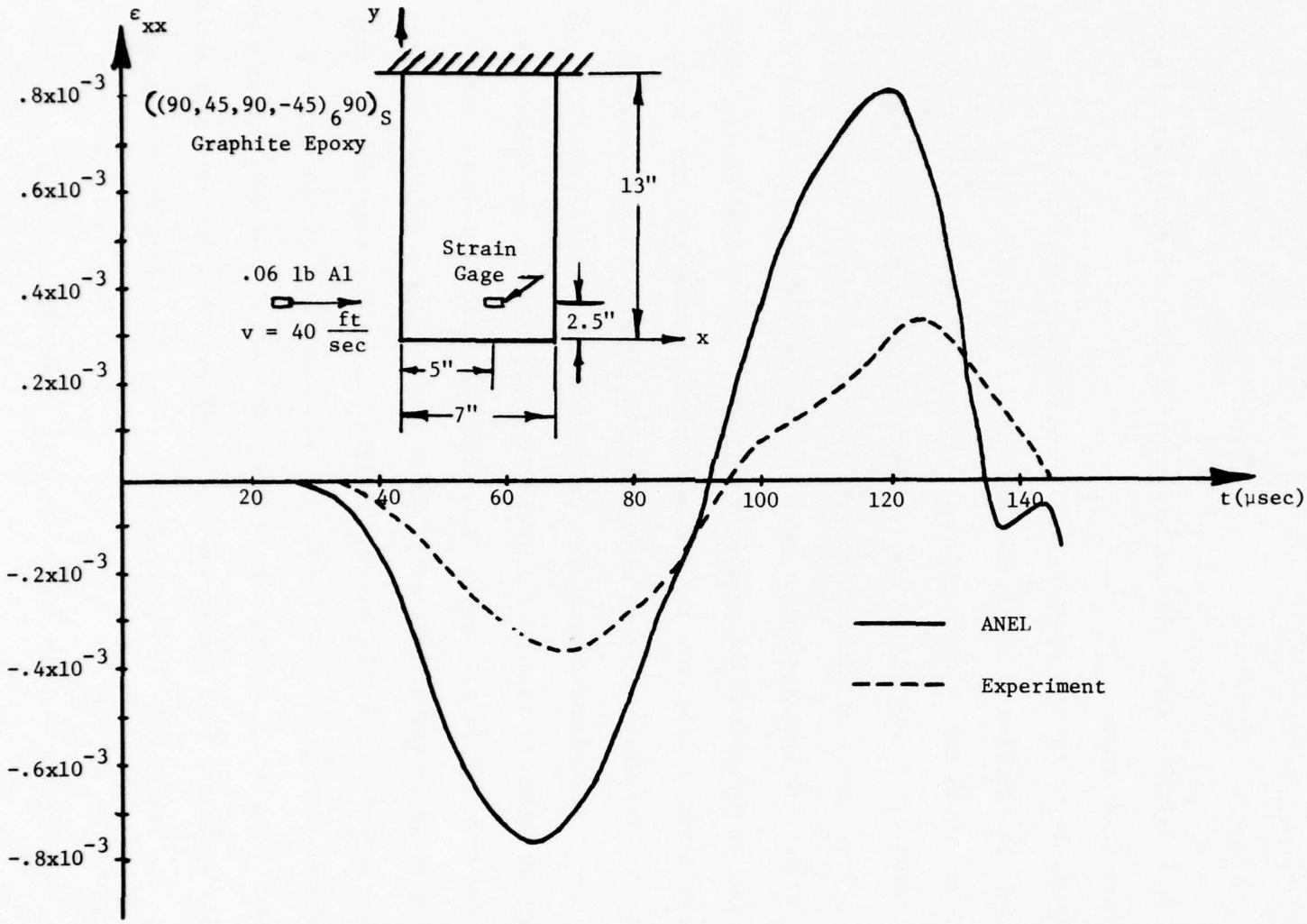

Figure 24. Comparison for Edge Impact of Composite Plate

it was a cylinder 2.54 cm long and 2.16 cm in diameter. The striking end of this projectile was rounded with a radius of 2.54 cm. Perhaps by using either the radius of the rounded end for the radius of the ball or the diameter of the cylinder for the diameter of the area of contact would have given a more realistic loading function. Another reason for the discrepancy between the computer study and experiment is that ANEL is a completely elastic code. No provision was made for the plastic deformation during impact. Likewise the energy dissipation and wave dispersion were not accounted for in ANEL. The wave propagates from the impact point to the strain gage in a "weak" direction of the laminated plate, i.e. it is 90° or 45° from the fiber direction; the wave is essentially travelling thru the matrix. It can be expected that the viscoelastic effect was strong and much of the energy was dissipated before reaching the gage.

Figure 25 shows a plot of the strain across the plate from the left hand edge to the right hand edge at y = 1.87 in. (4.75 cm) and t = 48 sec. The strain that occurs at the left hand edge on this curve is the maximum value of strain occurring in the 140 μsec for which ANEL was run. As seen the strain decreases as one moves across the plate from left to right.

In summary one can say that ANEL tends to give higher readings than experiment but does model the shape of the wave fairly accurately. More work must be done with the code in order to introduce plasticity. Also some additional study must be performed because in the plane stress case of ANEL some numerical anomaly appears at the free boundary. However, as ANEL exists now, one can say that the program does at least give conservative results.

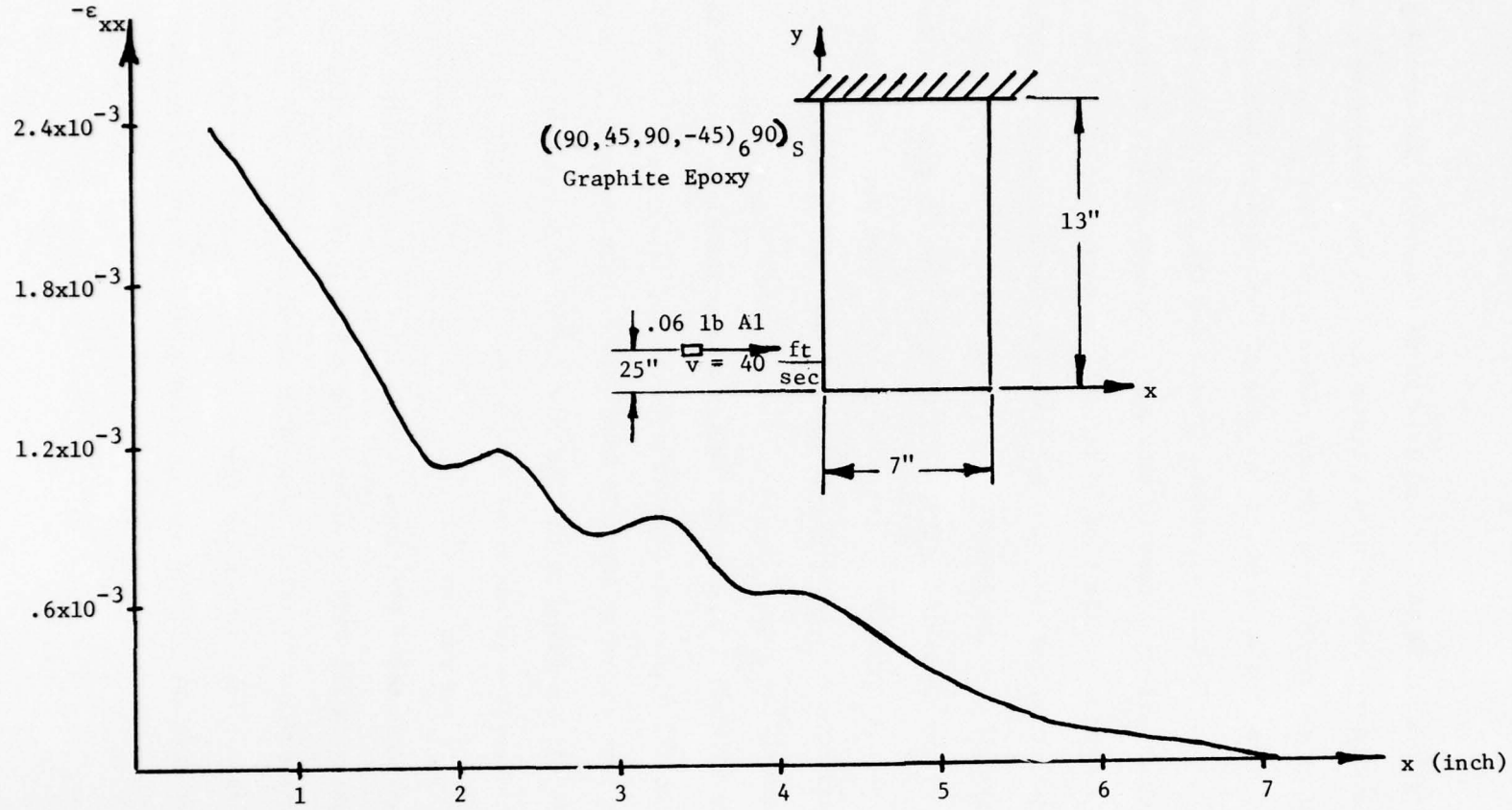

Figure 25. Strain Distribution Across Composite Plate at y = 1.87 in. and t = 48 μsec. Maximum Strain at x = 0.47 in., y = 1.87 in., t = 48 μsec.

APPENDIX A

STATIC SOLUTION OF A SIMPLY SUPPORTED ORTHOTROPIC PLATE

In this appendix, we will present the details of the derivation of the constants K_1 and d_{12} for the central transverse impact of a simply supported orthotropic plate. As explained in the main text, these constants are needed for developing the design curve.

The static deflection of such a plate due to an arbitrary load distribution p(x,y) is [A1],

$$w(x,y) = \sum_{m=1}^{\infty} \sum_{n=1}^{\infty} \frac{p_{mn} \sin \frac{m\pi x}{a} \sin \frac{n\pi y}{b}}{\frac{m^4\pi^4}{a^4} D_x + 2H \frac{m^2n^2\pi^4}{a^2b^2} + \frac{n^4\pi^4}{b^4} D_y} \tag{A1}$$

where $$H = \nu_y D_x + 2D_{xy}$$

and

$$p_{mn} = \frac{4}{ab} \int_0^b \int_0^a p(x,y) \sin \frac{m\pi x}{a} \sin \frac{n\pi y}{b} \, dxdy$$

For a centrally applied point load P,

$$p_{mn} = \frac{4P}{ab} \sin \frac{m\pi}{2} \sin \frac{n\pi}{2}$$

The maximum deflection occuring at the center of the plate is,

$$w_1 = w\left(\frac{a}{2}, \frac{b}{2}\right) = \sum_{m=1,3,5}^{\infty} \sum_{n=1,3,5}^{\infty} \frac{4P_{ab}}{\pi^4 D_x} \left(\frac{a}{b}\right)^2 \frac{1}{C_{mn}}$$

where

$$C_{mn} = m^4 + 2m^2n^2 \left(\frac{a}{b}\right)^2 \frac{H}{D_x} + n^4 \left(\frac{a}{b}\right)^4 \frac{D_y}{D_x}$$

We will assume that

$$H = \sqrt{D_x D_y} \tag{A2}$$

so that

$$C_{mn} = m^4 + 2m^2n^2\eta + n^4\eta^2 \tag{A3}$$

where
$$\eta = \left(\frac{a}{b}\right)^2 \sqrt{\frac{D_y}{D_x}} \tag{A4}$$

Therefore, recalling that

$$K_1 = P/w_1$$

we have

$$K_1 = \frac{\pi^4 D_x}{4ab\left(\frac{a}{b}\right)^2 f_1(\eta)} \tag{A5}$$

where

$$f_1(\eta) = \sum_{m=1,3,5}^{\infty} \sum_{n=1,3,5}^{\infty} \frac{1}{C_{mn}} \tag{A6}$$

The tensile strain in the x-direction due to bending is

$$\varepsilon_x = - z \frac{\partial^2 w}{\partial x^2}$$

which will have its maximum value at

$$(x,y,z) = (a/2,\ b/2,\ h/2)$$

We will derive the relationship between the strain at this point ε_2 and the maximum deflection.

$$\varepsilon_2 = - \frac{h}{2} \left.\frac{\partial^2 w}{\partial x^2}\right|_{x=a/2, y=b/2}$$

$$= \frac{2Ph}{\pi^2 D_x} \left(\frac{a}{b}\right) f_2(\eta) \tag{A7}$$

where

$$f_2(\eta) = \sum_{m=1,3,5}^{\infty} \sum_{n=1,3,5}^{\infty} \frac{m^2}{C_{mn}}$$

Substituting for P, we obtain

$$\varepsilon_2 = \frac{2K_1 h}{\pi^2 D_x} \left(\frac{a}{b}\right) f_2(\eta)\ w_1$$

so that

$$d_{12} = \frac{\pi^2 D_x}{2K_1 h\ (a/b)\ f_2(\eta)} \tag{A8}$$

The approximation assumption used above, Eq. (A2), has been suggested by Timoshenko and Woinowsky-Krieger [A1] for simplifying the mathematics of several plate-bending problems and is exact for the case of an isotropic plate. The advantage of this assumption is to reduce the parameters for describing the geometry and anisotropy of the plate to a single quantity, η. For the composite plate on which the impact experiments were performed, the computed values are

$$H = D_{12} + 2D_{66} = 13140 \text{ lb-in.}$$

and $$\sqrt{D_x D_y} = \sqrt{D_{11} D_{22}} = 11517 \text{ lb-in.}$$

a difference of 14%.

Reference

A1. Timoshenko, S., and Woinowsky-Krieger, S., Theory of Plates and Shells, Second Edition, McGraw-Hill Co., New York, 1959

APPENDIX B

COMPUTER PROGRAM FOR CALCULATING TIMOSHENKO SOLUTION OF PLATE IMPACT

This appendix presents a listing of the FORTRAN computer program, named SMINC3, for calculating the Timoshenko small-increment solution of the central transverse impact of a rectangular orthotropic plate, Eq. (29).

The program as listed is set up to solve an impact problem having the following parameters:

$v = 2.45$ m/sec

axbxh = 171 x 349 x 7.1 mm

$m_1 = 0.660$ kg

$m_2 = 0.816$ kg

The plate bending stiffnesses, computed according to the Whitney-Pagano anisotropic plate theory [9], arè:

$D_{11} = 680.4$ N-m

$D_{12} = 473.2$ N-m

$D_{22} = 2488.8$ N-m

$D_{66} = 505.7$ N-m

$D_{16} = D_{26} = -49.1$ N-m

$A_{44} = A_{55} = 2.687 \times 10^7$ N/m

The plate is treated as orthotropic and the D_{16} and D_{26} terms are neglected.

The program itself calculates the value of the Hertzian contact stiffness constant based on supplied values of isotropic elastic properties of the plate and impactor. The values used are:

plate (Gr/Ep) $\begin{cases} E = 9.8 \times 10^9 \text{ N/m}^2 \\ \nu = 0.3 \end{cases}$

impactor (steel) $\begin{cases} E = 2.1 \times 10^{11} \text{ N/m}^2 \\ \nu = 0.33 \end{cases}$

The contact radius of the impactor is 25.4 mm.

```
C      SMINC3  --  PLATE IMPACT
COMPUTATION OF TIMOSHENKO-TYPE SMALL-INCREMENT SOLUTION OF HERTZIAN
C     IMPACT OF A SIMPLY SUPPORTED ORTHOTROPIC RECTANGULAR PLATE
C      MODIFIED SUN & CHATTOPADHYAY METHOD
C      DT = TIME INCREMENT
C      NDT = NO. OF TIME INCREMENTS CALCULATED
C      TOL = TOLERANCE OF ERROR IN NONLINEAR SOLUTION
C      V = IMPACT VELOCITY
C      XA, YB, H = DIMENSIONS OF PLATE IN X, Y, Z DIRECTIONS
C      M1, M2 = MASS OF PLATE, IMPACTOR
C      E1, E2 = ELASTIC MODULUS OF PLATE, IMPACTOR
C      PR1, PR2 = POISSON'S RATIO OF PLATE, IMPACTOR
C      NHM, NHN = NUMBER OF VIBRATION MODES CONSIDERED
C      K2 = HERTZIAN CONTACT STIFFNESS
C      XNX, YNY = INITIAL STRESSES IN X,Y DIRECTIONS
       REAL L,M1,M2,K2,L11,L12,L13,L22,L23,L33
       DIMENSION F(5000),GW(5000),GXX(5000),GYY(5000)
C********    PROBLEM DATA    ***********************************************
       NHM=25
       NHN=25
       NDT=100
       TOL=1.0E-05
       DT=1.0E-06
       XNX=0.
       YNY=0.
       D11=680.4
       D12=473.2
       D22=2488.6
       D66=505.7
       A44=2.687E 07
       A55=A44
       XNX=0.
       YNY=0.
       XA=0.171
       YB=0.349
       H=0.0071
       M1=0.660
       M2=0.816
       R1=0.0254
       PR1=0.3
       PR2=0.33
       E1=9.8E 09
       E2=2.10E 11
       V=2.45
C*************************************************************************
       Z=H/2.
       PI=3.14159265398
 1001 FORMAT(4X,"N",8X,"TIME",14X,"FORCE",12X,"APPROACH",10X,"DEFLECTION
     1",10X,"STRAIN X",10X,"STRAIN Y",10X,"STRAIN XY")
       DEL1=(1.-PR1**2)/E1/PI
       DEL2=(1.-PR2**2)/E2/PI
       K2=4.*SQRT(R1)/(DEL1+DEL2)/PI/3.
       CAY=PI**2/12.
       A44=A44*CAY
       A55=A55*CAY
       B=DT**2/3.0/M2
        C= 4.0/M1
       P=M1/XA/YB
```

```
      PRINT1001
CALCULATE NATURAL FREQUENCIES OF PLATE
      DO90K=1,NDT
      GW(K)=0.
      GXX(K)=0.
   90 GYY(K)=0.
      DO247M=1,NHM,2
      TERMA=M*PI/XA
      TERMA2=TERMA**2
      L13=A55*TERMA
      DO247N=1,NHN,2
      TERMB=N*PI/YB
      TERMB2=TERMB**2
      L11=D11*TERMA2+ D66*TERMB2+A55
      L12=(D12+D66)*TERMA*TERMB
      L22=D66*TERMA2+D22*TERMB2+A44
      L23=A44*TERMB
      L33=(A55+XNX)*TERMA2+(A44+YNY)*TERMB2
      Q=L11*L22-L12**2
      DETERM=Q*L33+2.*L12*L23*L13-L22*L13**2-L11*L23**2
      AC=(L12*L23-L22*L13)/Q*TERMA
      BC=(L12*L13-L11*L23)/Q*TERMB
      OMEGA2=DETERM/Q/P
      OMEGA=SQRT(OMEGA2)
      IF((M.EQ.1).AND.(N.EQ.1))PRINT1002,OMEGA
 1002 FORMAT("    OMEGA,1,1 = ",E15.8)
      TERM1=DT*OMEGA
      C2=1.0
      DO247K=1,NDT
      C1=C2
      C2=COS(K*TERM1)
      AAA=(C1-C2)/OMEGA2
CONSTRUCT TABLES OF SUMMATION FUNCTIONS
      GW(K)=GW(K)+AAA
      GXX(K)=GXX(K)+AAA*AC
  247 GYY(K)=GYY(K)+AAA*BC
      P=B+C*GW(1)
      Q=1./3.
      S=2./3.
      DO100N=1,NDT
CREATE HEADINGS FOR DATA AT TOP OF EVERY PAGE
      IF(MOD(N,61).NE.0)GOTO70
 1003 FORMAT(1H1)
      PRINT1003
      PRINT1001
   70 T=N*DT
      A=V*T
      IF(N.EQ.1)GOTO14
      BUM=0.
      NM1=N-1
      SUMI=0.
      SUM=0.
      DO5J=1,NM1
      K=N-J
      R=K
      SUM1=F(J)-SUMI
      SUM=SUM+R*SUM1
    5 BUM=BUM+F(J)*GW(K+1)
```

```
      A=A-C*BUM
      A=A-DT**2*(2.*SUM-SUMI/3.)/M2
C COMPUTE SOLUTION FOR F(N) USING NEWTON"S ITERATIVE METHOD
      GOTO13
   14 FNEW=SQRT(A**3)/K2
   13 FN=FNEW
      B=SIGN(1.0,FN)/K2**2-3.0*A*P**2
      FFN=P**3*FN**3+B*FN**2
     1  +3.0*A**2*P*FN-A**3
      FPFN=3.0*P**3*FN**2+2.0*B*FN+3.0*A**2*P
   82 FNEW=FN-FFN/FPFN
      ERROR=ABS((FNEW-FN)/FN)
      IF(ERROR.GT.TOL)GOTO13
      IF(N.GT.1)GOTO10
C CHECK THAT F(1) IS POSITIVE
      IF(FNEW.GT.0.)GOTO10
      FNEW=-FNEW
      GOTO13
   10 F(N)=FNEW
      IF(FNEW.LT.0.)F(N)=0.
C CALCULATE STRAIN AND DEFLECTION
      W=0.
      PSIXX=0.
      PSIYY=0.
      DO21J=1,N
      K=N-J+1
      W=W+F(J)*GW(K)
      PSIXX=PSIXX+F(J)*GXX(K)
   21 PSIYY=PSIYY+F(J)*GYY(K)
      W=W*C
      EPSX=-PSIXX*C*Z
      EPSY=-PSIYY*C*Z
      GAMMA=0.
      ALPHA=SIGN(1.0,FNEW)*(ABS(FNEW)/K2)**S
      PRINT1000,N,T,F(N),ALPHA,W,EPSX,EPSY,GAMMA
  100 CONTINUE
      STOP
 1000 FORMAT(1X,I4,7(3X,E15.8))
      END
```

APPENDIX C

COEFFICIENTS FOR THE PLANE-STRESS CASE

The terms containing the coefficients A,B,C,D,E,F,G,R, and T in the conservation-of-mass equation (43) and the strain-rate equations (44)-(47) are different from zero only for the plane-stress case. They result from the plane-stress assumptions, i.e., the stress components σ_{13}, σ_{23}, and σ_{33} equal to zero and there is no variation in stress or strain in the direction perpendicular to the plane (i.e. the x_3 direction). The relationship between stress and strain is

$$\sigma_{ij} = C_{ijk\ell}\, \varepsilon_{k\ell}$$

Now since σ_{13}, σ_{23}, and σ_{33} are zero, one can solve for ε_{33}, ε_{13}, and ε_{23} in terms of ε_{11}, ε_{12}, and ε_{22} and get

$$\varepsilon_{33} = A\, \varepsilon_{11} + B\, \varepsilon_{22} + C\, \varepsilon_{12}$$
$$\varepsilon_{13} = D\, \varepsilon_{11} + E\, \varepsilon_{22} + F\, \varepsilon_{12}$$
$$\varepsilon_{23} = G\, \varepsilon_{11} + R\, \varepsilon_{22} + T\, \varepsilon_{12}$$

These coefficients are in terms of the stiffness constants $C_{ijk\ell}$. Chou and Carleone [16] have compiled these coefficients for various material symmetries. For instance an orthotropic material will have

$$A = -\frac{C_{3311}}{C_{3333}} \qquad B = -\frac{C_{3322}}{C_{3333}}$$

$$C = D = F = G = R = T = 0$$

APPENDIX D

DERIVATION OF CONSTITUTIVE RELATIONS

This appendix gives the derivation of the constitutive relations (52) and (53) which are in terms of the deviator stress and deviator strain, from the familiar generalized Hooke's Law in terms of total stress σ and strain ε. The generalized Hooke's law is

$$\sigma_{ij} = C_{ijk\ell}\, \varepsilon_{k\ell} \tag{D-1}$$

where $C_{ijk\ell}$ are the stiffness constants of the anisotropic elastic material. (See for instance [16] and [17])

The deviator stress S and the deviator strain e are given as follows:

$$S_{ij} = \sigma_{ij} - \sigma_m\, \delta_{ij} \tag{D-2}$$

$$e_{ij} = \varepsilon_{ij} - \varepsilon_m\, \delta_{ij} \tag{D-3}$$

where

$$\sigma_m = \frac{1}{3}\, \sigma_{\ell\ell} \tag{D-4}$$

$$\varepsilon_m = \frac{1}{3}\, \varepsilon_{\ell\ell} \tag{D-5}$$

Note all indices assume values 1, 2, and 3.

Performing a tensor contraction on Eq. (D-1) gives

$$\sigma_{ii} = C_{iik\ell}\, \varepsilon_{k\ell}. \tag{D-6}$$

Making a substitution of $\varepsilon_{k\ell}$ from Eq. (D-3) and a substitution of σ_{ii} from Eq. (D-4), Eq. (D-6) then becomes

$$\sigma_m = \frac{1}{3}\left[C_{iik\ell}\, e_{k\ell} + C_{iikk}\, \varepsilon_m\right] \tag{D-7}$$

Let us now substitute Eqs. (D-2) and (D-3) into Eq. (D-1). After some rearranging the following is obtained

$$S_{ij} + \sigma_m\, \delta_{ij} = C_{ijk\ell}\, e_{k\ell} + C_{ijkk}\, \varepsilon_m \tag{D-8}$$

Substituting for σ_m in Eq. (D-8) from Eq. (D-7) gives

$$S_{ij} = \frac{1}{3}\left[3\,C_{ijk\ell} - C_{qqk\ell}\,\delta_{ij}\right] e_{k\ell} + \frac{1}{3}\left[3\,C_{ijkk} - C_{qqkk}\,\delta_{ij}\right] \varepsilon_m \tag{D-9}$$

Now taking the total time derivative along a particle path of Eqs. (D-9) and (D-7) gives

$$\frac{\mathcal{D}S_{ij}}{\mathcal{D}t} = \frac{1}{3}\left[3\,C_{ijk\ell} - C_{qqk\ell}\,\delta_{ij}\right] \dot{e}_{k\ell} \frac{1}{3}\left[3\,C_{ijkk} - C_{qqkk}\,\delta_{ij}\right] \dot{\varepsilon}_m \tag{D-10}$$

$$\frac{D\sigma_m}{Dt} = \frac{1}{3}\left[C_{iik\ell}\,\dot{e}_{k\ell} + C_{iikk}\,\dot{\varepsilon}_m\right] \tag{D-11}$$

where $\mathcal{D}/\mathcal{D}t$ is the Jaumann derivative that has been discussed in the main body of the report.

Eqs. (D-10) and (D-11) are Eqs. (52) and (53) respectively.

REFERENCES

1. Noh, W.F., 'CEL: Coupled Eulerian-Lagrange Code', in Methods of Computational Physics, Vol. 3, edited by Alder, B.; Fernbach, S.; and Rotenburg, M.; Academic Press, New York, 1964.

2. Maenchen, G. and Sack, S., 'The Tensor Code', in Methods of Computational Physics, Vol. 3, edited by Alder, B.; Fernbach, S.; and Rotenburg, M.; Academic Press, New York, 1964.

3. Hageman, L.J., and Walsh, J.M., "HELP, A Multi-Material Eulerian Program for Compressible Fluid and Elastic-Plastic Flows in Two Space Dimensions and Time', Ballistics Research Laboratories, Aberdeen Proving Ground, Maryland, Contract Report No. 39, May 1971.

4. Wilkins, Mark L., 'Calculation of Elastic-Plastic Flow', University of California, Lawrence Radiation Laboratory, Report UCRL-7322, April, 1963.

5. Chou, P.C., and Flis, W.J., "Design Curves for Structural Response Due to Impact Loading," presented at the AIAA/ASME/SAE 17th Structures, Structural Dynamics, and Materials Conference, King of Prussia, Pa., May 5-7 1976.

6. Timoshenko, S.P., "Zur Frage nach der Wirkung eines Stosses auf einen Balken," Z. Math. Phys., Vol. 62, 1913, No. 2, pp. 198-209.

7. Karas, K., "Platten Unter Seitlichen Stoss," Ingenieur-Archiv, Vol. 10, 1939, p. 237.

8. Sun, C.T., and Chattopadhyay, S., "Dynamic Response of Anisotropic Laminated Plates Under Initial Stress to Impact of a Mass," Trans. ASME, J. Appl. Mech., Vol. 42, 1975, p. 693.

9. Whitney, J.M., and Pagano, N.J., "Shear Deformation in Heterogeneous Anisotropic Plates," Trans. ASME, J. Appl. Mech., Vol. 37, 1970, p. 1031.

10. Karpp, Robert R., 'Accuracy of HEMP Code Solutions', Ballistic Research Laboratories, Aberdeen Proving Ground, Maryland, Memorandum Report No. 2268, January, 1973.

11. Giroux, E.D., 'HEMP User's Manual', Lawrence Livermore Laboratory, University of California, Livermore, California, UCRL-51079 Rev. 1, Dec. 17, 1973.

12. Jaumann, G., Sitzungsberichte Akad, Wiss., Wien (IIa), 1911.

13. Malvern, Lawrence E., Introduction to the Mechanics of a Continuous Medium, Prentice-Hall, Inc., Englewood Cliffs, N.J., 1969.

14. Greszczuk, L.B., 'Response of Isotropic and Composite Materials to Particle Impact', Foreign Object Impact Damage to Composites, ASTM STP 568, American Society for Testing and Materials, 1975, pp. 183-211.

15. Goldsmith, Werner, Impact: The Theory and Physical Behavior of Colliding Solids, E. Arnold, 1960, pp. 82-91.

16. Chou, Pei Chi and Carleone, Joseph, 'An Introduction to Anisotropic Elasticity', Mechanics and Structures Advanced Study Group, Drexel University, Phila., Pa. Report No. 71-14, September, 1971.

17. Lekhnitskii, S.G., Theory of Elasticity of an Anisotropic Elastic Body, Holden-Day, San Francisco, 1963.

LIST OF SYMBOLS

a = plate dimension in x-direction

b = plate dimension in y-direction

c_0 = beam flexural wave velocity = $\sqrt{E/\rho}$

c_1 = plate flexural wave velocity = $\sqrt{D_{11}/I}$

D_{ij} = plate flexural stiffness matrix

e = effective mass factor

EI = flexural rigidity of beam

F = contact force

h = depth of beam

k = radius of gyration

k_2 = Hertzian contact stiffness

K_1 = eqivalent beam spring constant

K_2 = linearized contact stiffness (spring constant)

L = length of beam

m_1 = mass of structure

m_2 = mass of impactor

M = m_1/m_2

P = static load

t = time

v = velocity of impactor before impact

v_0 = initial velocity immediately after impact

w = $w(x,t)$ = beam deflection

(= $w(x)$ = static beam deflection)

= $w_1(x)$ = deflection of structure at impact point

w_{1max} = maximum midspan deflection

w_2 = $w_2(t)$ = displacement of impactor

x = beam axial coordinate

z = distance from beam neutral axis

α = contact approach = $w_2 - w_1$

δ = static midspan deflection of beam

ε = $\varepsilon(t)$ = strain at midspan

ε_{max} = maximum value of (t)

$\bar{\varepsilon}$ = generalized strain

ρA = linear density of beam

ϕ = density of fluid

☆ U. S. GOVERNMENT PRINTING OFFICE: 1977 — 757-001/287